

Survey of Gravitationally-lensed Objects in HSC Imaging (SuGOHI). VI. Crowdsourced lens finding with Space Warps.

Alessandro Sonnenfeld^{1,2*}, Aprajita Verma³, Anupreeta More^{2,4}, Campbell Allen³, Elisabeth Baeten⁵, James H. H. Chan⁶, Roger Hutchings³, Anton T. Jaelani^{7,8}, Chien-Hsiu Lee⁹, Christine Macmillan⁵, Philip J. Marshall¹⁰, James O' Donnell³, Masamune Oguri^{2,11,12}, Cristian E. Rusu¹³, Marten Veldthuis³, Kenneth C. Wong^{2,14}, Claude Cornen⁵, Christopher P. Davis¹⁰, Adam McMaster³, Laura Trouille¹⁵, Chris Lintott³, and Grant Miller³

¹ Leiden Observatory, Leiden University, Niels Bohrweg 2, 2333 CA Leiden, the Netherlands
e-mail: sonnenfeld@strw.leidenuniv.nl

² Kavli IPMU (WPI), UTIAS, The University of Tokyo, Kashiwa, Chiba 277-8583, Japan

³ Sub-department of Astrophysics, University of Oxford, Denys Wilkinson Building, Keble Road, Oxford OX1 3RH, UK

⁴ The Inter-University Center for Astronomy and Astrophysics, Post bag 4, Ganeshkhind, Pune, 411007, India

⁵ Zooniverse, c/o Astrophysics Department, University of Oxford, Oxford

⁶ Institute of Physics, Laboratory of Astrophysics, École Polytechnique Fédérale de Lausanne (EPFL), Observatoire de Sauverny, 1290 Versoix, Switzerland

⁷ Department of Physics, Kindai University, 3-4-1 Kowakae, Higashi-Osaka, Osaka 577-8502, Japan

⁸ Astronomy Study Program and Bosscha Observatory, FMIPA, Institut Teknologi Bandung, Jl. Ganesha 10, Bandung 40132, Indonesia

⁹ National Optical Astronomy Observatory 950 N Cherry Avenue, Tucson, AZ 85719, USA

¹⁰ Kavli Institute for Particle Astrophysics and Cosmology, Stanford University, 452 Lomita Mall, Stanford, CA 94035, USA

¹¹ Department of Physics, University of Tokyo, 7-3-1 Hongo, Bunkyo-ku, Tokyo 113-0033, Japan

¹² Research Center for the Early Universe, University of Tokyo, 7-3-1 Hongo, Bunkyo-ku, Tokyo 113-0033, Japan

¹³ Subaru Telescope, National Astronomical Observatory of Japan, 2-21-1 Osawa, Mitaka, Tokyo 181-0015, Japan

¹⁴ National Astronomical Observatory of Japan, 2-21-1 Osawa, Mitaka, Tokyo 181-8588, Japan

¹⁵ Adler Planetarium, Chicago, IL, 60605, USA

ABSTRACT

Context. Strong lenses are extremely useful probes of the distribution of matter on galaxy and cluster scales at cosmological distances, but are rare and difficult to find. The number of currently known lenses is on the order of 1,000.

Aims. We wish to use crowdsourcing to carry out a lens search targeting massive galaxies selected from over 442 square degrees of photometric data from the Hyper Suprime-Cam (HSC) survey.

Methods. We selected from the S16A internal data release of the HSC survey a sample of $\sim 300,000$ galaxies with photometric redshifts in the range $0.2 < z_{\text{phot}} < 1.2$ and photometrically inferred stellar masses $\log M_* > 11.2$. We crowdsourced lens finding on this sample of galaxies on the Zooniverse platform, as part of the Space Warps project. The sample was complemented by a large set of simulated lenses and visually selected non-lenses, for training purposes. Nearly 6,000 citizen volunteers participated in the experiment. In parallel, we used YATTALENS an automated lens finding algorithm, to look for lenses in the same sample of galaxies.

Results. Based on a statistical analysis of classification data from the volunteers, we selected a sample of the most promising $\sim 1,500$ candidates which we then visually inspected: half of them turned out to be possible (grade C) lenses or better. Including lenses found by YATTALENS or serendipitously noticed in the discussion section of the Space Warps website, we were able to find 14 definite lenses (grade A), 129 probable lenses (grade B) and 581 possible lenses. YATTALENS found half the number of lenses discovered via crowdsourcing.

Conclusions. Crowdsourcing is able to produce samples of lens candidates with high completeness and purity, compared to currently available automated algorithms. A hybrid approach, in which the visual inspection of samples of lens candidates pre-selected by discovery algorithms and/or coupled to machine learning is crowdsourced, will be a viable option for lens finding in the 2020s with forthcoming wide area surveys such as LSST, Euclid and WFIRST.

Key words. Gravitational lensing: strong – Galaxies: elliptical and lenticular, cD

1. Introduction

Strong gravitational lensing is a very powerful tool for galaxy evolution and cosmology. For example, strong lenses have been used to study the inner structure of galaxies and its evolution (e.g. Treu & Koopmans 2002; Koopmans & Treu 2003; Auger et al. 2010; Ruff et al. 2011; Bolton et al. 2012; Sonnenfeld

et al. 2013b), to put constraints on the stellar initial mass function (IMF) of massive galaxies (e.g. Treu et al. 2010; Spiniello et al. 2012; Barnabè et al. 2013; Smith et al. 2015; Sonnenfeld et al. 2019) and on their dark matter content (e.g. Sonnenfeld et al. 2012; Newman et al. 2015; Oldham & Auger 2018). Strong lensing is a unique tool for detecting the presence of substructure inside, or along the line of sight of, massive galaxies (e.g. Mao & Schneider 1998; More et al. 2009; Vegetti et al. 2010;

* Marie Skłodowska-Curie Fellow

Hsueh et al. 2019). Strongly lensed compact sources, such as quasars or supernovae, have been used to measure the surface mass density in stellar objects via the microlensing effect (e.g. Mediavilla et al. 2009; Schechter et al. 2014; Oguri et al. 2014), and to measure cosmological parameters from time delay observations (e.g. Suyu et al. 2016; Grillo et al. 2018; Wong et al. 2019; Millon et al. 2019). While very useful, strong lenses are rare, as they require the chance alignment of a light source with a foreground object with sufficiently large surface mass density. The number of currently known strong lenses is on the order of a thousand, the exact number depending on the purity of the sample¹. Despite this seemingly large number, the effective sample size is in practice much smaller for many strong lensing applications, once the selection criteria for obtaining suitable objects for a given study are applied. For example, most known lens galaxies have redshifts $z < 0.5$, limiting the time range that can be explored in evolution studies. For this reason, many strong lensing-based inferences are still dominated by statistical uncertainties due to small sample sizes. Expanding the sample of known lenses would therefore broaden the range of investigations that can be carried out, providing statistical power that is presently lacking.

Current wide-field photometric surveys, such as the Hyper Suprime-Cam Subaru Strategic Program (HSC SSP Aihara et al. 2018; Miyazaki et al. 2018), the Kilo Degree Survey (KiDS de Jong et al. 2015) and the Dark Energy Survey (DES Dark Energy Survey Collaboration et al. 2016) are allowing the discovery of hundreds of new promising strong lens candidates (Sonnenfeld et al. 2018; Petrillo et al. 2019a; Jacobs et al. 2019a, e.g.). Although details vary between surveys, the general strategy adopted to find new lenses consists in scanning images of galaxies with the potential of being lenses, given their mass and redshift, and looking for the presence of strongly lensed features around them. Due to the large areas covered by the aforementioned surveys (the HSC SSP is planned to acquire data over 1,400 square degrees of sky), the number of galaxies to be analysed in order to obtain a lens sample as complete as possible can easily reach the hundreds of thousands. In order to deal with such large numbers, the lens finding task is usually automated, either by making use of a lens finding algorithm or artificial neural networks trained on simulated data (see Metcalf et al. 2019, for an overview of some of the latest methods employed for lens finding in purely photometric data). We point out how current implementations of automatic lens finding algorithms, including those based on artificial neural networks, require some degree of visual inspection: typically these methods are applied in such a way as to prioritise completeness, resulting in a relatively low purity. For example, out of 1,480 lens candidates found by the algorithm YATTALENS in HSC data, only 46 were labelled as highly probable lens candidates (Sonnenfeld et al. 2018). Similarly, the convolutional neural networks developed by Petrillo et al. (2019a) for a lens search in KiDS data produced a list of 3,500 candidates, of which only 89 were recognised to be strong lenses with high confidence after visual inspection. Nevertheless, Petrillo et al. (2019a) showed how high purity can still be achieved without human intervention, although only with a great loss in completeness.

While it is both desirable and plausible that future improvements in the development of lens finding algorithms will lead to higher purity and completeness in lens searches, a currently

viable and very powerful approach to lens finding is crowdsourcing, harnessing the skill and adaptability of human pattern recognition. With crowdsourcing, lens candidates are distributed among a large number of trained volunteers for visual inspection. The Space Warps collaboration has been pioneering this method and applied it successfully to data from the Canada-France-Hawaii Telescope Legacy Survey (Marshall et al. 2016; More et al. 2016, CFHT-LS). In this work, we use crowdsourcing and the tools developed by the Space Warps team to look for strong lenses in 442 square degrees of imaging data collected from the HSC survey.

We obtained cutouts around $\sim 300,000$ massive galaxies selected with the criteria listed above and served them for inspection to a team of citizen scientist volunteers, together with training images consisting of known lenses, simulated lenses and non-lens galaxies, via the Space Warps platform. The volunteers were asked to simply label each image as either a lens or a non-lens. After collecting multiple classifications for each galaxy in the sample, we combined them, in a Bayesian framework, to obtain a probability for an object to be a strong lens. The science team then visually inspected the most likely lens candidates and classified them with more stringent criteria. In parallel to crowdsourcing, we searched for strong lenses in the same sample of massive galaxies by using the software YATTALENS, which has been used for past lens searches in HSC data (Sonnenfeld et al. 2018; Wong et al. 2018). By merging the crowdsourced lens candidates with those obtained by YATTALENS, we were able to discover a sample of 143 high probability lens candidates. Most of these very promising candidates were successfully identified as such by the citizens.

The aim of this paper is to describe the details of our lens finding effort, present the sample of newly discovered lens candidates, discuss the relative performance of crowdsourcing and of the YATTALENS software and to suggest strategies for future searches. The structure of this work is as follows. In Sect. 2, we describe the data used for the lens search, including the training set for crowdsourcing. In Sect. 3, we describe the setup of the crowdsourcing experiment and the algorithm used for the analysis of the classifications from the citizen scientist volunteers. In Sect. 4, we show our results, including the sample of candidates found with YATTALENS and highlighting interesting lens candidates of different types. In Sect. 5, we discuss the merits and limitations of the two lens finding strategies. We conclude in Sect. 6. All images are oriented with North up and East left.

2. The data

2.1. The parent sample

Our lens finding effort was based on a targeted search, as opposed to a blind one: we looked for lensed features among a set of galaxies based on the properties that make them potential lenses. Specifically, we targeted galaxies in the redshift range $0.2 < z < 1.2$ and with stellar mass M_* larger than $10^{11.2} M_\odot$, with photometric data from the HSC survey. The upper redshift and lower stellar mass bounds are a compromise between the will to obtain a sample of lenses as complete as possible and the need to keep the number of galaxies to be inspected by the volunteers within a reasonable value, while the lower redshift cut was introduced to avoid dealing with galaxies too bright for the detection of lensed features, which are typically faint. In order to select such a sample, we relied on the photometric redshift catalogue from the S16A internal data release of the HSC survey (Tanaka et al. 2018). In particular, we used data prod-

¹ More than half of the systems considered for this estimate are candidates with high probability of being lenses, but no spectroscopic confirmation.

ucts obtained with the template fitting-based photometric redshift software MIZUKI (Tanaka 2015), which fits explicitly and self-consistently for the star formation history of a galaxy and its redshift, using the five bands of HSC (g, r, i, z, y). We applied the redshift and stellar mass cuts listed above to the median value of the photometric redshift and the stellar mass provided by MIZUKI, for each galaxy with photometric data in all five HSC bands and detections in at least three bands, regardless of depth. We removed galaxies with saturated pixels, as well as probable stars, by setting $i_extendedness_value > 0$ and by removing objects brighter than 21 mag in i -band and a moments-derived size smaller than $0.4''$. Typical statistical uncertainties are 0.02 on the photo- z and 0.05 on $\log M_*$.

The steps described above led us to a sample of $\sim 300,000$ galaxies. From these, we removed 70 known lenses from the literature, mostly from our previous searches (Sonnenfeld et al. 2018; Wong et al. 2018; Chan et al. 2019), as well as a few hundred galaxies already inspected and identified as possible lenses (grade C candidates in our notation) in the aforementioned studies. Many of the known lenses were used for training purposes, as will be explained in subsection 3.1. The Sonnenfeld et al. (2018) search covered the same area as the present study, but targeted exclusively $\sim 43,000$ luminous red galaxies with spectra from the Baryonic Oscillation Spectroscopic Survey. Only about half of those galaxies belong to the sample used for our study, while the remaining half was excluded because of our stellar mass limit. Finally, we removed from the sample $\sim 4,000$ galaxies used as negative (i.e. non-lens) training subjects². The selection of these objects will be described in subsection 3.1. The final sample size consisted of 288,109 subjects.

2.2. Image preparation

We used g, r, i -band data from HSC S17A³ to produce RGB images for the candidate classification by the volunteers. S17A data was processed with the HSC data reduction pipeline HSCPIPE version 5.4 (Bosch et al. 2018), a version of the Large Synoptic Survey Telescope stack (Ivezić et al. 2008; Axelrod et al. 2010; Jurić et al. 2015). We obtained 101×101 pixel (i.e. $17.0 \times 17.0''$) cutouts from coadded and sky-subtracted data in each band, then produced versions of these data with the light from the main (foreground) galaxy subtracted off. The main purpose for foreground (putative lens galaxy) subtraction was to facilitate the detection of faint lensed features that would normally be blended with the lens light. Foreground light subtraction was carried out by fitting a Sérsic surface brightness profile to the data, using YATTALENS. The structural parameters of the Sérsic model (e.g. the half-light radius, position angle, etc.) were first optimised on the i -band data (the band with the best image quality), then a scaled-up version of the model, convolved with the model point spread function (PSF) produced by HSCPIPE, was subtracted off from the data in each band. The presence of lens light-subtracted images was one of the main elements of novelty in our experiment, compared to past searches with Space Warps, which, in fact, recommended the adoption of such a procedure to improve the detection of lenses.

The original and foreground-subtracted data were used to make two sets of RGB images, with different colour schemes.

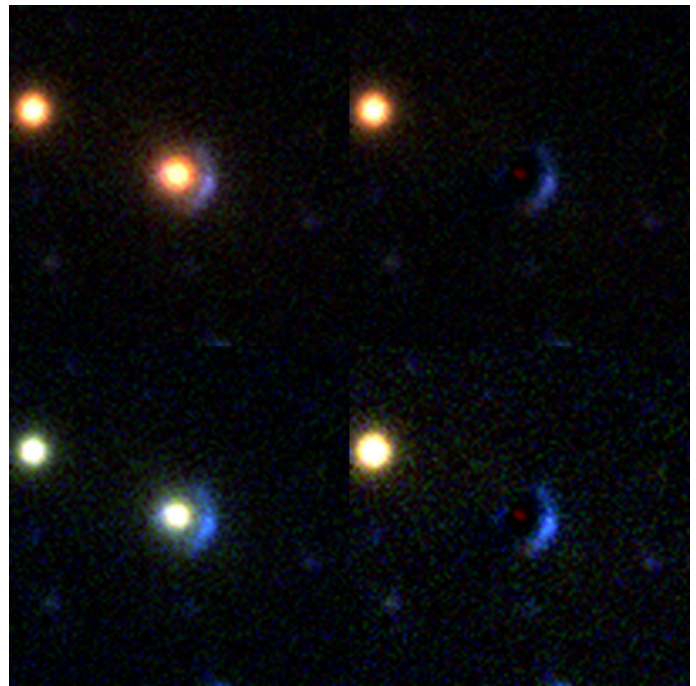


Fig. 1. Colour-composite HSC images of lens SL2SJ021411–040502. Images with the light from the foreground galaxy subtracted are shown on the right, while original images are on the left. The images at the top and bottom row were created with the ‘standard’ and ‘optimal’ colour schemes, respectively.

All colour schemes were based on a linear mapping between the flux in each pixel and the intensity in the 8-bit RGB channel of the corresponding band:

$$\begin{aligned} R &= 255 \times \min(i/i_{\text{cut}}, 1), \\ G &= 255 \times \min(r/r_{\text{cut}}, 1), \\ B &= 255 \times \min(g/g_{\text{cut}}, 1). \end{aligned} \quad (1)$$

In the above equations, i, r, g indicate the flux in each band, while $i_{\text{cut}}, r_{\text{cut}}$ and g_{cut} are threshold values: pixels with higher flux than these thresholds are assigned the maximum allowed intensity, 255. In a similar vein, pixels with negative flux are given 0 intensity. In the first colour scheme, dubbed ‘standard’, we fixed $i_{\text{cut}}, r_{\text{cut}}$ and g_{cut} for all images, set to sufficiently low values so as to make it possible to detect objects with surface brightness close to the background noise level. This choice resulted in images with consistent colours for different targets, though often with saturated centres, especially for the brightest galaxies. We also adopted a second colour scheme, named ‘optimal’, where we used a dynamical definition of the threshold flux for each subject: in the original image (i.e. without foreground subtraction), this was set to the 99%-ile of the pixel values in each band, so that the main galaxy, typically the brightest object in the cutout, was not saturated, except for the very central pixels. The ‘optimal’ threshold flux of the foreground-subtracted images was instead set to the minimum between the 90%-ile of the residual image and the flux corresponding to ten times the sky background fluctuation. We made this choice to highlight features close to the background noise level. As an example, we show the aforementioned four versions of the RGB images of a known lens, SL2SJ021411–040502, in Fig. 1.

² The term subject refers to cutouts centred on our target galaxies.

³ S17A is a more recent data release than S16A, on which the target selection was based. While reduced data from S17A were available at the start of our experiment, the photo- z catalogue was not, hence the use of an earlier release to define the sample of targets.

3. Crowdsourcing experiment setup

Our crowdsourcing project, named “Space Warps - HSC”, was hosted on the Zooniverse⁴ platform. The setup of the experiment followed largely that of previous Space Warps efforts, with minor modifications. We summarise it here, but refer to Marshall et al. (2016) for further details.

Upon landing on the Space Warps website⁵, volunteers were presented with two main options: reading a brief documentation on the basic concepts of gravitational lensing, or moving directly to the image classification phase. The documentation included various examples of typical strong lens configurations, as well as false positives: non-lens galaxies with lens-like features such as spiral arms or star-forming rings and typical image artefacts. During the image classification phase, volunteers were shown sets of four images of individual subjects, of the kind of Fig. 1, and asked to decide whether the subject showed any signs of gravitational lensing, in which case they were asked to click on the image, or else proceed to the next subject. On the side of the classification interface, a ‘Field Guide’ with a summary of various lens types and common impostors was always available for volunteers to consult. Users accessing the image classification interface for the first time were guided through a brief tutorial, which summarised the goals of the crowdsourcing experiment, the basics of gravitational lensing and the classification submission procedure.

In addition to the documentation, the ‘Field Guide’ and the tutorial, we relied on training images to help volunteers sharpen their classification skills. Participants were shown subjects, to be graded, interleaved with training images of lenses (known or simulated), known as ‘sims’ for simplicity, or of non-lens galaxies, referred to as ‘duds’. They were not told whether a subject was a training one until after they submitted their classification, when a positive or negative feedback message was displayed, depending on whether they guessed the correct nature of the subject (lens or non-lens) or not (with some exceptions, described later). Training images were interleaved in the classification stream with a frequency of one in three for the first 15 subjects shown, reducing to one in five for the next 25 subjects and then settling to a rate of one in ten as volunteers became more experienced. The sims and duds were randomly served throughout the experiment to each registered volunteer. As the number of sims was 50% higher than the duds in the training subject pool, the sims were shown with correspondingly higher frequency than the duds. We describe in detail the properties of the training images in subsection 3.1.

Volunteers also had the opportunity to discuss the nature of individual subjects on the ‘Talk’ (i.e. forum) section of the Space Warps website: after deciding the class of a subject, clicking on the “Done & Talk” button would submit the classification and prompt the volunteer to a dedicated forum page, where they could leave comments on it, ask questions and view any previous related discussion. Volunteers did not have the possibility of changing their classification once it was submitted, so the main purposes of this forum tool was to give them a chance to bring the attention on specific subjects and ask for opinions from other volunteers or experts. This helped the volunteers in building a better understanding of gravitational lensing, as well as creating a sense of community. We regularly browsed ‘Talk’ to answer questions and to look for outstanding subjects highlighted by volunteers.

Volunteer classifications were compiled and analysed using the Space Warps Analysis Pipeline (Marshall et al. 2016, *SWAP*) to obtain probabilities of each subject being a lens. We describe *SWAP* in subsection 3.2, and in practice used a modified version of the implementation of *SWAP* written for the Zooniverse platform by Michael Laraia et al.⁶

3.1. The training sample

Training subjects served three different purposes. The first was helping volunteers to learn how to distinguish lenses from non-lenses, as discussed above. The second purpose was to keep volunteers alert through pop-up boxes that give real-time feedback on their classifications of the training images: given that the fraction of galaxies that are strong lenses in real data is very low, showing long uninterrupted sequences of subjects could have led volunteers to adopt a default non-lens classification, which could have resulted in the mis-classification of the rare, but extremely valuable, real lenses. The third purpose was allowing us to evaluate the accuracy of the classifications by volunteers, so as to adjust the weight of their scores in the calculation of the lens probabilities of subjects (more details will follow in subsection 3.2). In order to serve these functions properly, it was crucial for training subjects to be as indistinguishable as possible from real ones. This required having a large number of them, so that volunteers could always be shown training images never seen previously⁷. We prepared images of thousands of training subjects of two classes: lenses and non-lens impostors.

3.1.1. The lens sample

Lens training subjects were, for the most part, simulated ones, generated by adding images of strongly lensed galaxies on top of HSC images of galaxies from the Baryon Acoustic Oscillations Survey (BOSS Dawson et al. 2013) luminous red galaxy samples. Our priority was to generate simulations covering as large a volume of parameter space as possible, within the realm of galaxy-scale lenses, in order not to bias volunteers against rare lens configurations. For this reason, rather than assuming a physical model, we imposed very loose conditions on the mapping between the observed properties of the galaxies selected to act as lenses and their mass distribution. Given a BOSS galaxy, we first assigned a lens mass profile to it, in the form of a singular isothermal ellipsoid (SIE Kormann et al. 1994). We drew the value of the Einstein radius θ_{Ein} from a uniform distribution in the range $0.5'' < \theta_{\text{Ein}} < 3.0''$. The lower limit was set to roughly match the resolution limit of HSC data (the typical i -band seeing is $0.6''$), while the upper limit was imposed to restrict the simulations to galaxy-scale lenses (as opposed to group- or cluster-scale lenses, which have typical Einstein radii of several arcseconds). We drew the lens mass centroid from a uniform distribution within a circle of one pixel radius, centred on the central pixel of the cutout (which typically coincides with the galaxy light centroid). We drew the axis ratio of the SIE from a uniform distribution between 0.4 and 1.0, while the orientation of

⁶ The modified *SWAP*-2 branch used here can be found at <https://github.com/cpadavis/swap-2> which is based on <https://github.com/miclaraia/swap-2>

⁷ In practice, due to some platform/image server issues, some volunteers saw a small fraction of training subjects more than once. However, only the first classification made by a user of any given subject was used in *SWAP*.

⁴ <https://www.zooniverse.org>

⁵ spacewarps.org

the major axis was drawn from a Normal distribution centred on the lens galaxy light major axis and with a 10 degree dispersion.

The background source was modelled with an elliptical Sérsic light distribution. Its half-light radius, Sérsic index and axis ratio were drawn from uniform distributions in the ranges $0.2'' - 3.0''$, $0.5 - 2.0$ and $0.4 - 1.0$, respectively, and its position angle was randomly oriented. We assigned source magnitudes in g, r, i bands to those of objects randomly drawn from the CFHTLenS photometric catalogue (Hildebrandt et al. 2012; Erben et al. 2013). The source position distribution was drawn from the following axi-symmetric distribution:

$$P(\theta_s) \propto \left(\frac{\theta_s}{\theta_{\text{Ein}}}\right) \exp\left\{-4\frac{\theta_s}{\theta_{\text{Ein}}}\right\}, \quad (2)$$

where θ_s is the radial distance between the source centroid and the centre of the image. The above distribution is approximately linear in θ_s at small radii, as one would expect for sources uniformly distributed in the plane of the sky, but then peaks at $\theta_{\text{Ein}}/4$ and turns off exponentially at large radii. The rationale for this choice was to down-weight the number of lenses with a very asymmetric image configuration, which correspond to values θ_s close to the radial caustic of the SIE lens (i.e. the largest allowed value of θ_s for a source to be strongly lensed), at an angular scale $\approx \theta_{\text{Ein}}$. Sources close to the radial caustic are lensed into a main image, subject to minimal lensing distortion, and a very faint (usually practically invisible) counter-image close to the centre. These systems are strong lenses from a formal point of view, but in practice are hard to identify as such. They would dominate the simulated lens population if we assumed a strictly uniform spatial distribution of sources, hence the alternative distribution of Eq. 2.

Not all lens-source pairs generated this way were strong lenses: in $\sim 13\%$ of cases the source fell outside the radial caustic. Such systems were simply removed from the sample. Among the remaining simulations, most showed clear signatures of strong lensing (e.g. multiple images and/or arcs). For some, however, it was difficult to identify them as lenses from visual inspection alone. We decided to include in the training sample all strong lenses, regardless of how obvious their lens nature was, so that volunteers would have the opportunity to learn how to identify lenses in the broadest possible range of configurations. This choice could also allow us to carry out a quantitative analysis of the completeness of crowdsourced lens finding as a function of a variety of lens parameters, although that is beyond the scope of this work.

We split the lens training sample in two categories: an ‘easy’ subsample, consisting of objects showing fairly obvious strong lens features, and a ‘hard’ subsample, consisting of less trivial lenses to identify visually. After classifying an easy lens, volunteers received a positive feedback message (“Congratulations! You spotted a simulated lens”) or a negative one (“Oops, you missed a simulated lens. Better luck next time!”), depending on whether they correctly identified it as a lens or not. For hard lenses, we used a different feedback rule: a correct identification still triggered a positive feedback message (“Congratulations! You’ve found a simulated lens. This was a tough one to spot, well done for finding it.”), but no feedback message was provided in case of misidentification, in order not to discourage volunteers with unrealistic expectations (often the lensed images in these hard sims were impossible to see at all). The implementation of two levels of feedback is a novelty of this study, compared to previous Space Warps experiments.

The separation of the lens training sample in easy and hard categories was based on the following algorithm, developed in a

few iterations involving the visual inspection of a small sample of simulated lenses. For each lens, we first defined the lensed source footprint as the ensemble of cutout pixels in which the source g -band flux exceeded the sky background noise by more than 3σ . We then counted the number of connected regions in pixel space, using the function LABEL from the MEASURE module of the Python SCIKIT-IMAGE package, and used it as a proxy for the number of images N_{img} . We also counted the number n_{visible} of ‘visible’ source pixels (not necessarily connected) where the source surface brightness exceeded that of the lens galaxy in the g -band. The latter was estimated from the best-fit Sérsic model of the lens light. Any subject with $n_{\text{visible}} < 40$ pixels or $N_{\text{img}} = 0$ was labelled as a hard one. Hard lenses were also systems with $N_{\text{img}} = 1$ but with a source footprint smaller than 100 pixels. Among lenses with $N_{\text{img}} > 1$, those with the footprints of the brightest and second brightest images smaller than 100 and 20 pixels respectively were also given a hard lens label. All other lenses were classified as easy. We converged to these values after inspecting a sample of simulated lenses, by making sure that the classification obtained with this algorithm matched our judgement of what constitutes an easy and a hard lens. We show examples of lenses from the two categories in Fig. 2. We generated a total of $\sim 12,000$ simulated lenses, to which we added 52 known lenses from the literature. About 60% of them were easy lenses.

Although the BOSS galaxies used as lenses are labelled as red, a substantial fraction of them are late-type galaxies, i.e. they exhibit spiral arms, disks or rings. Simulations with a late-type galaxy as a lens are more difficult to recognise, because the colours of the lensed images is often similar to those of star-forming regions in the lens galaxy. Nevertheless, we allowed late-type galaxies as lenses in the training sample, as we did not want to bias the volunteers against this class of objects.

3.1.2. The non-lens sample

The most difficult aspect of lens finding through visual inspection is distinguishing true lenses, intrinsically rare, from non-lens galaxies with lens-like features such as spiral arms or, more generally, tangentially elongated components with different colours from those of the main galaxy body. The latter are much more common than the former, so any inaccuracy in the classification has typically a large impact on the purity of a sample of lens candidates. In order to maximise opportunities for volunteers to learn how to differentiate between the two categories, we designed our duds training set by including exclusively non-lens objects bearing some degree of resemblance to strong lenses.

We searched for suitable galaxies among a sample of $\sim 6,600$ lens candidates identified by YATTALENS, which we ran over the whole sample of subjects before starting the crowdsourcing experiment. Details on the lens search with the YATTALENS algorithm will be given in subsection 4.2. Upon visual inspection, a subset of $\sim 3,800$ galaxies were identified as unambiguous non-lenses and deemed suitable for training purposes. These were used as our sample of duds. We show examples of duds in Fig. 3. In order to double the number of available duds, we also included in the training set versions of the original duds rotated by 180 degrees.

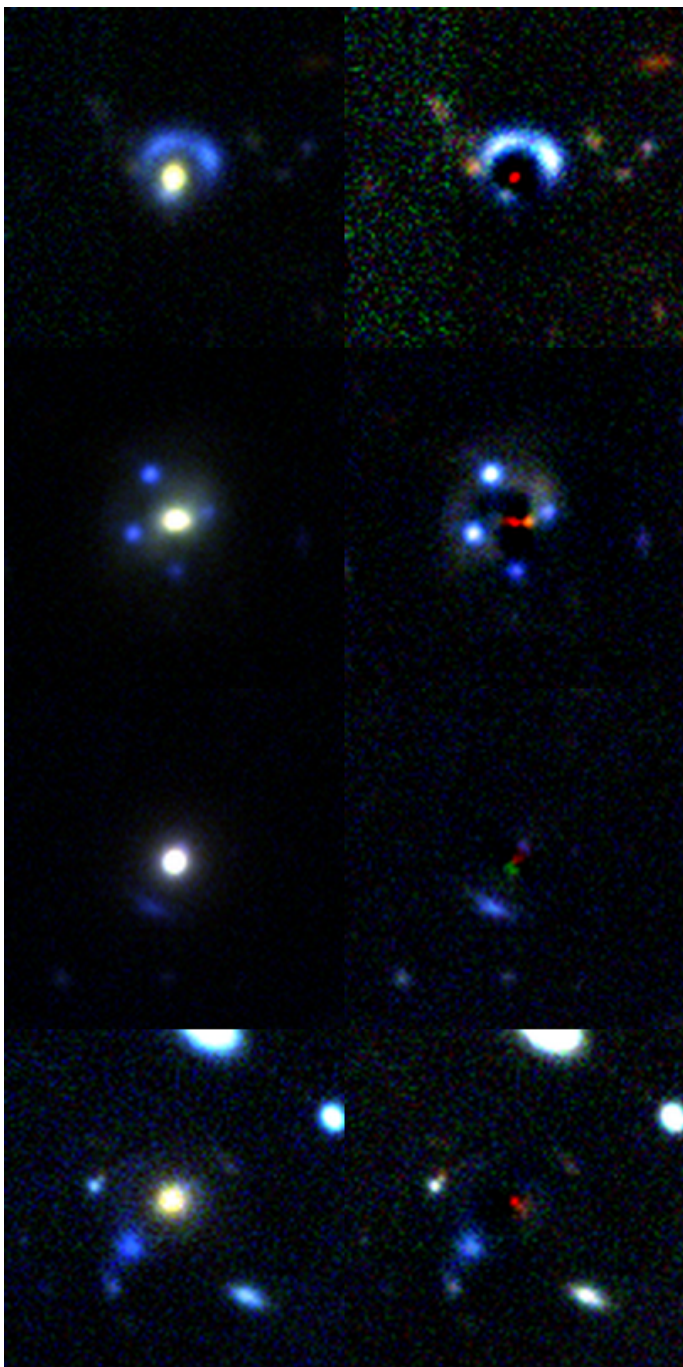


Fig. 2. Set of four simulated lenses, rendered using the “optimised” colour scheme, with and without foreground subtraction. The first two lenses from the top are labelled as easy, while the bottom two are examples of hard lenses.

3.2. The classification analysis algorithm

The SWAP algorithm was introduced and discussed extensively by Marshall et al. (2016). We summarise here its main concepts. The goal of the crowdsourcing experiment is to quantify, for each subject, the posterior probability of it being a lens, given the data, $P(\text{LENS}|\mathbf{d})$. The data used for the analysis consisted of the ensemble of classifications from all users who have seen the subject. This included, for the k -th user, the classification on the subject itself, C_k , as well as past classifications on training

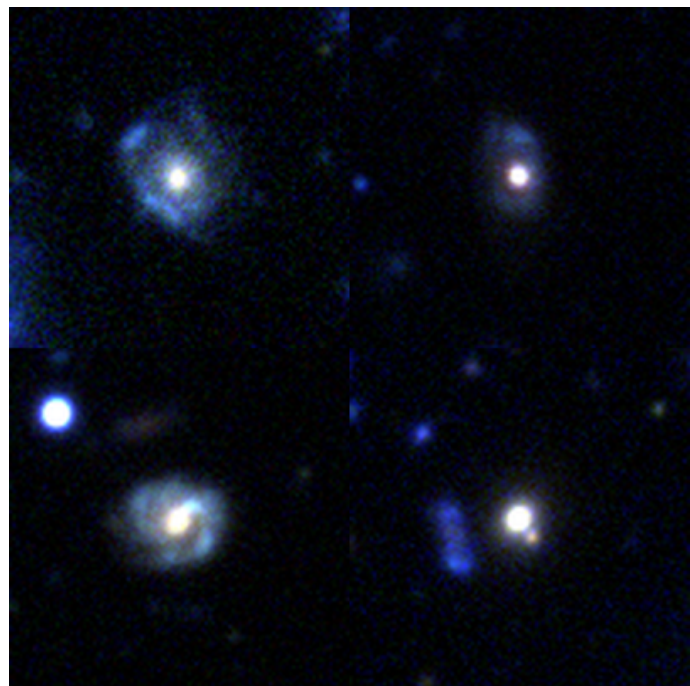


Fig. 3. Set of four non-lens duds from the training set, rendered using the “optimised” colour scheme.

subjects \mathbf{d}_k^t :

$$\mathbf{d} = (\{C_k\}, \{\mathbf{d}_k^t\}), \quad (3)$$

where curly brackets denote ensembles over all volunteers who have classified the subject and the classification C_k can take the values ‘LENS’ or ‘NOT’.

Using Bayes’ theorem, the posterior probability of a subject being a lens given the data is

$$P(\text{LENS}|\{C_k\}, \{\mathbf{d}_k^t\}) = \frac{P(\text{LENS})P(\{C_k\}|\text{LENS}, \{\mathbf{d}_k^t\})}{P(\{C_k\}|\{\mathbf{d}_k^t\})}, \quad (4)$$

where $P(\text{LENS})$ is the prior probability of a subject being a lens, $P(\{C_k\}|\text{LENS}, \{\mathbf{d}_k^t\})$ is the likelihood of obtaining the ensemble of classifications given that the subject is a lens and given the past classifications of volunteers on training subjects, while $P(\{C_k\}|\{\mathbf{d}_k^t\})$ is the probability of obtaining the classifications, marginalised over all possible subject classes:

$$P(\{C_k\}|\{\mathbf{d}_k^t\}) = P(\{C_k\}|\text{LENS}, \{\mathbf{d}_k^t\})P(\text{LENS}) + P(\{C_k\}|\text{NOT}, \{\mathbf{d}_k^t\})P(\text{NOT}). \quad (5)$$

Before any classification takes place, the posterior probability of a subject being a lens is equal to its prior, which we assume to be

$$P(\text{LENS}) = 2 \times 10^{-4}, \quad (6)$$

loosely based on estimates from past lens searches in CFHT-LS data. Although our HSC data is slightly better than CFHT-LS both in terms of image quality and depth, which should correspond in principle to a higher fraction of lenses, we do not expect that to make a significant difference. This is because, as we will clarify later, we designed our experiment so that the final posterior probability of a subject is always dominated by the likelihood and not by the prior.

After the first classification is made, C_1 , we update the posterior probability, which becomes

$$P(\text{LENS}|C_1, \mathbf{d}_1^t) = \frac{P(\text{LENS})P(C_1|\text{LENS}, \mathbf{d}_1^t)}{P(C_1|\mathbf{d}_1^t)}. \quad (7)$$

We evaluate the likelihood based on past performance of the volunteer on training subjects. We approximate the probability of the volunteer correctly classifying a lens subject with the rate at which they did so on training subjects:

$$P(\text{'LENS'}|\text{LENS}, \mathbf{d}_1^t) \approx \frac{N_{\text{'LENS'}}$$

where N_{LENS} is the number of sims the volunteer classified and $N_{\text{'LENS'}}$ the number of times they classified these sims as lenses. Given that 'LENS' and 'NOT' are the only two possible choices, the probability of the same volunteer wrongly classifying a lens as a non-lens is

$$P(\text{'NOT'}|\text{LENS}, \mathbf{d}_1^t) = 1 - P(\text{'LENS'}|\text{LENS}, \mathbf{d}_1^t). \quad (9)$$

Similarly, we approximate the probability of a volunteer correctly classifying a dud as

$$P(\text{'NOT'}|\text{NOT}, \mathbf{d}_1^t) \approx \frac{N_{\text{'NOT'}}$$

Let us now consider a subject for which k classifications from an equal number of volunteers have been gathered. If a $k+1$ -th classification is collected, we can use the posterior probability of the subject being a lens after the first k classifications, $P(\text{LENS}|C_1, \dots, C_k, \mathbf{d}_1^t, \dots, \mathbf{d}_k^t)$, as a prior for the probability of the subject being a lens before the new classification is read. The posterior probability of the subject being a lens after the $k+1$ th classification then becomes:

$$\frac{P(\text{LENS}|C_{k+1}, \mathbf{d}_{k+1}^t, C_1, \dots, C_k, \mathbf{d}_1^t, \dots, \mathbf{d}_k^t)}{P(\text{LENS}|C_1, \dots, C_k, \mathbf{d}_1^t, \dots, \mathbf{d}_k^t)P(C_{k+1}|\text{LENS}, \mathbf{d}_{k+1}^t)}, \quad (11)$$

where the probability of observing a classification C_{k+1} , the denominator of the above equation, is

$$\begin{aligned} P(C_{k+1}|\mathbf{d}_{k+1}^t) = \\ P(C_{k+1}|\text{LENS}, \mathbf{d}_{k+1}^t)P(\text{LENS}|C_1, \dots, C_k, \mathbf{d}_1^t, \dots, \mathbf{d}_k^t) + \\ P(C_{k+1}|\text{NOT}, \mathbf{d}_{k+1}^t)P(\text{NOT}|C_1, \dots, C_k, \mathbf{d}_1^t, \dots, \mathbf{d}_k^t). \end{aligned} \quad (12)$$

Eq. 11 allows us to update the probability of a subject being a lens every time a new classification is submitted.

As shown in past Space Warps experiments, after a small number of classifications is collected (typically 11 for a lens and 4 for a non-lens), $P(\text{LENS}|\mathbf{d})$ almost always converges to either very low values, indicating that the subject is most likely not a lens, or to values very close to unity, suggesting that the subject is a lens (see e.g. Figure 5 of Marshall et al. 2016). The posterior probability is in either case very different from the prior, indicating that the likelihood terms are driving the inference. In order to make the experiment more efficient, we retired subjects (i.e. we stopped showing them to the volunteers) when they reached a lens probability smaller than 10^{-5} after at least 4 classifications: gathering additional classifications would not have changed the probability of those subjects significantly, and removing them from the sample allowed us to prioritise subjects with fewer classifications. Regardless of $P(\text{LENS}|\mathbf{d})$, we retired subjects after 30 classifications were collected. In practice, SWAP was not run

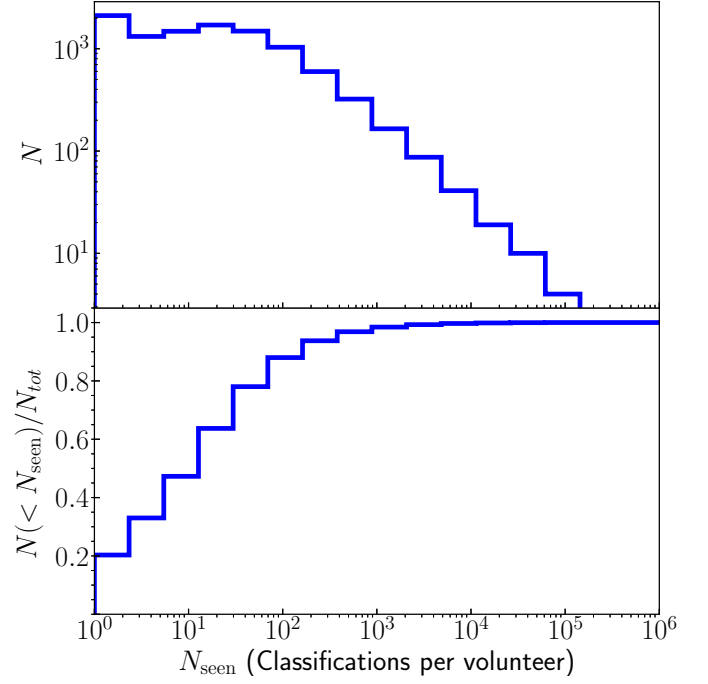


Fig. 4. *Top:* Distribution in the number of classified subjects per volunteer. *Bottom:* cumulative distribution.

continuously, but only every 24 hours. This caused minor inconsistencies between the retirement rules described above and the subjects being shown to the volunteers. These inconsistencies, along with other unreported issues such as the retirement server being offline and due to delayed release of subjects, did slightly reduce the overall efficiency of the experiment but these did not affect the probability analysis.

4. Results

4.1. Search with Space Warps

The Space Warps - HSC crowdsourcing experiment was launched on April 27, 2018. It saw the participation of $\sim 6,000$ volunteers, who carried out 2.5 million classifications over a period of two months. With the goal of assessing the degree of involvement of the volunteers, we show in Fig. 4 the distribution in the number of classified subjects per user, N_{seen} . This is a declining function of N_{seen} , typical of crowdsourcing experiments: while most volunteers classified less than twenty subjects, nearly 20% of them contributed each with at least a hundred classifications. It is thanks to these highly committed volunteers that the vast majority of the classifications needed for our analysis was gathered.

In Fig. 5, we show the distribution of lens probabilities of the full sample of subjects (thick blue histograms), as quantified with the SWAP software. This is a highly bimodal distribution: most of the subjects have very low lens probabilities, as expected, given the rare occurrence of the strong lensing phenomenon, but there is a high probability peak, corresponding to the objects identified as lenses by the volunteers. We then made an arbitrary cut at $P(\text{LENS}) = 0.5$: 1,577 subjects with a lens probability larger than this value were declared 'promising candidates' and promoted to the next step in our analysis, which consisted of visual inspection by the experts in strong lensing. This further refinement of the lens candidate sample will be described in detail in subsection 4.3.

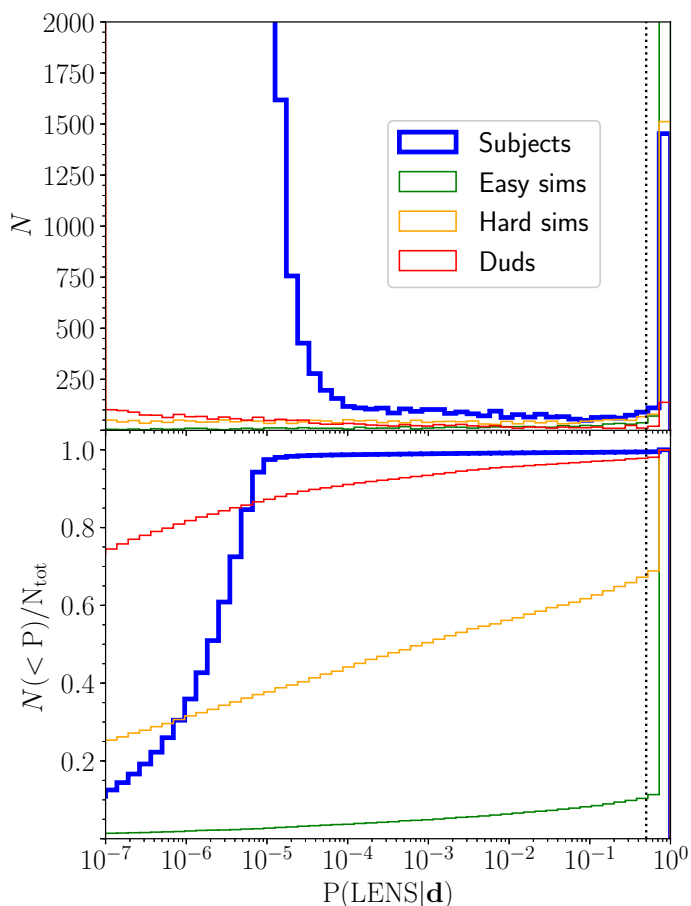


Fig. 5. *Top:* Distribution in the posterior probability of subjects, duds and sims being lenses, given the classification data from the volunteers. *Bottom:* cumulative distribution. The vertical dotted line marks the limit above which subjects are declared promising candidates and promoted to the expert visual inspection step.

In Fig. 5 we also plot the distributions in lens probability of the three sets of training subjects: duds, easy sims and hard sims. These follow roughly our expectations: most of the duds are correctly identified as such, 90% of the easy lenses have $P(\text{LENS}) > 0.5$, while only a third of the hard lenses make it into our promising candidate cut. This validates our set of choices and criteria that went into compiling the easy and hard sims. Of the 52 known lenses used for training, 49 were successfully classified as lenses (not shown in Fig. 5). The 3 missed ones were all hard lenses.

4.2. Search with YATTALENS

YATTALENS is a lens finding algorithm developed by Sonnenfeld et al. (2018), consisting of two main steps. In the first step, it runs SExtractor (Bertin & Arnouts 1996) on foreground light-subtracted g -band images to look for tangentially elongated images (i.e. arcs) and possible counter-images with similar colours. In the second step, it fits a lens model to the data and compared the goodness-of-fit with that obtained from two alternative non-lens models. In case the lens model fits best, it keeps the system as a candidate strong lens.

We ran YATTALENS on the sample of $\sim 300,000$ galaxies obtained by applying the stellar mass and photometric redshift cuts described in subsection 2.1 to the S16A internal data release catalogue of HSC. More than 90% of the subjects were discarded

at the arc detection step. Of the remaining $\sim 22,000$, 6,779 were flagged as possible lens candidates by YATTALENS and the rest was discarded on the basis of the lens model not providing a good fit. We then visually inspected the sample of lens candidates with the purpose of identifying non-lenses erroneously classified by YATTALENS that could be used for training purposes. The $\sim 3,800$ galaxies that made up the duds were drawn entirely from this sample.

4.3. Lens candidate grading

We merged the sample of lens candidates identified by the volunteers, 1,577 subjects with $P(\text{LENS}|\mathbf{d}) > 0.5$, with the YATTALENS sample, from which we removed the $\sim 3,800$ subjects used as duds.

We also added to the sample 264 outstanding candidates flagged by volunteers on the ‘Talk’ section of the Space Warps website, which we browsed on a roughly daily basis, quickly inspecting subjects with recent comments (typically on the order of a few tens each day). This last subsample is by no means complete (we did not systematically inspect all subjects flagged by the volunteers) and has a large overlap with the set of probable lenses produced by the classification algorithm. Nevertheless, we included it in order to make sure that potentially interesting candidates would not get lost. Although most of the candidates inspected in this way turned out not to be lenses, this step still proved to be useful, because it enabled the discovery of a few lenses that would have otherwise been missed (as we will show later).

We then visually inspected the resulting sample with the purpose of refining the candidate classification. Nine co-authors of this paper assigned to each candidate an integer score from 0 to 3, to indicate the likelihood of the subject being a strong lens. We used the following scoring convention:

- Score = 3: almost certainly a lens. A textbook example for which all characteristics of lensed images are verified: image configuration, consistency of colour and, in case of extended sources, surface brightness among all images. Additionally, the possibility of lensed features being the result of contamination can be ruled out with high confidence.
- Score = 2: probably a lens. All of the features match those expected for a strong lens, but the possibility that some of the features are due to contaminants cannot be ruled out.
- Score = 1: possibly a lens. Most of the features are consistent with those expected for a strong lens, but they may as well be explained by contaminants.
- Score = 0: almost certainly not a lens. Features are inconsistent with those expected for a strong lens.

Additionally, in order to ensure consistency in grading criteria across the whole sample and among different graders, we proposed the following algorithm for assigning scores.

1. Identify the images that could be lensed counterparts of each other
2. Depending on the image multiplicity and configuration, assign an initial score as follows:
 - Einstein rings, sets of four or more images, sets consisting of at least one arc and a counter-image: 3 points.
 - Sets of three or two images, single arcs: 2 points.
3. If the lens is a clear group or cluster, add an extra point up to a maximum provisional score of 3.

Table 1. Number of lens candidates of grades of each grade found among subjects selected by the cut $P(\text{LENS}|\mathbf{d}) > 0.5$, from the ‘Talk’ section of Space Warps, by YATTALENS and in the merged sample.

Sample	A	B	C	0	# Inspected
$P(\text{LENS} \mathbf{d}) > 0.5$	14	118	465	980	1577
‘Talk’	11	84	121	48	264
YATTALENS	6	67	233	6473	6779
Merged	14	129	581	7152	7876

- Remove points based on how likely it is that the observed features are the result of contamination or image artefacts: if artefacts are present, then multiple images may not preserve surface brightness, may show mismatch of colours or may have the wrong orientation or curvature around the lens galaxy.
- Make sure that the final score is reasonable, given the definitions outlined above.

The rationale for the third point is to take into account the fact that a) groups and clusters are more likely to be lenses, due to their high mass concentration, and b) often produce non-trivial image configurations which might be penalised during the fourth step. Finally, we averaged the scores of all nine graders, and assigned a final grade as follows:

- Grade A: $\langle \text{Score} \rangle > 2.5$.
- Grade B: $1.5 < \langle \text{Score} \rangle \leq 2.5$.
- Grade C: $0.5 < \langle \text{Score} \rangle \leq 1.5$.
- Grade 0: $\langle \text{Score} \rangle \leq 0.5$.

We found 14 grade A lenses, 129 grade B and 581 C lens candidates. In Table 1 we provide a summary of the number of lens candidates of each grade found separately by Space Warps, both from the selection based on classification data and from the ‘Talk’ section, and with YATTALENS.

The first thing we can see from Table 1 is that, among the 724 lens candidates with grade C and above (sum of the first three columns in the bottom row), 597 of them (82%) are in the sample of subjects with $P(\text{LENS}|\mathbf{d}) > 0.5$. Only 11 of the 129 grade B candidates and none of the grade A ones were missed by the analysis of volunteer classification data (i.e. have $P(\text{LENS}|\mathbf{d}) \leq 0.5$). In contrast, only about half of the grade A, B and C candidates were flagged as possible lenses by YATTALENS. This clearly indicates that crowdsourcing returned a relatively more complete sample of candidates compared to YATTALENS. We will discuss this and other differences in performance between the two methods in subsection 5.1.

In Table 2 we list all the grade A and B candidates discovered. The full list of lens candidates with grade C and better is provided online, in our database containing all lens candidates found or analysed by SuGOHI⁸. This database was created by merging samples of lenses from our previous studies. Lens candidates that have been independently discovered as part of different lens searches can have different grades, because of differences in the photometric data used for grading, including the size and colour scheme of the image cutouts, or in the composition of the team who performed the visual inspection. In such cases, the higher grade was taken, under the assumption that it was driven by a higher quality in the image cutout used for the inspection (in terms of the lensed features being more clearly visible). As

⁸ <http://www-utap.phys.s.u-tokyo.ac.jp/~oguri/sugohi/>
Candidates from this study are identified by the value ‘SuGOHI6’ in the ‘Reference’ field.

a result, the number of grade A and B lens candidates from this study present in the SuGOHI database is slightly larger than the 143 candidates listed in Table 2. This is due to an overlap between the lens candidates found in this work and those from our visual inspection of galaxy clusters by Jaelani et al. (2020, , Paper V), carried out in parallel.

One of the main goals of this experiment was to extend the sample of known lenses to higher lens redshifts. In Fig. 6, we plot a histogram with the distribution in photo- z of our grade A and B lens candidates, together with candidates from our previous searches and compared to the lens redshift distribution from other surveys. The SuGOHI sample consists now of 324 highly probable (grade A or B) lens candidates. This is comparable to strong lens samples found in the Dark Energy Survey (DES, where Jacobs et al. 2019b, discovered 438 previously unknown lens candidates, one of which is also in our sample) and in the Kilo-Degree Survey (KiDS: Petrillo et al. 2019b, presented ~ 300 new candidates, not shown in Figure 6 due to a lack of published redshifts, 15 of which are also in our sample). Most notably, 41 of our lenses have photo- z s larger than 0.8, which is more than any other survey.

Some caution is required when using photometric redshifts, though: the distribution in photo- z of all our subjects (shown as a dashed histogram in Fig. 6) shows unusual peaks around a few values, which appear to reflect in the photo- z distribution of the lenses (dotted line). Given the large sky area covered by our sample, we would have expected a much smoother photo- z distribution. We therefore think these peaks to be the result of systematic errors in the photo- z . In order to obtain an estimate for the magnitude of such errors, we considered the subset of galaxies from our sample with spectroscopic redshift measurements from the literature (see Tanaka et al. 2018, for details on the spectroscopic surveys overlapping with HSC). The distribution in spectroscopic redshift of galaxies with photo- z larger than 1.0 has a median value of 1.05 and a tail that extends towards low redshifts. The 10%-ile of this distribution is at a spectroscopic redshift of 0.65. Assuming that the distribution in spectroscopic redshift of the lens sample follows a similar distribution, we can use this as a lower limit to the true redshift of our $z_{\text{phot}} > 1.0$ candidates. Since we are not using photo- z information to perform any physical measurement, we defer any further investigation of photo- z systematics to future studies.

4.4. A diverse population of lenses

In the rest of this section, we highlight a selected sample of lens candidates that we find interesting, grouped by type. We begin by showing in Fig. 7 a set of eight lenses with a compact background source, i.e. lenses with images that are visually indistinguishable from a point source. Compact strongly lensed sources are interesting because they could be associated with active galactic nuclei, or alternatively could be used to measure the sizes of galaxies that would be difficult to resolve otherwise (see e.g. More et al. 2017; Jaelani et al. 2019). The two lenses in the top row of Fig. 7 were also featured in the fourth paper of our series, dedicated to a search for strongly lensed quasars (Chan et al. 2019). All lenses shown in Fig. 7 were classified as such by the volunteers (the value of $P(\text{LENS}|\mathbf{d})$ is shown in the top left corner of each image), with the exception of HSCJ091843–022007. We were able to include it in our sample thanks to a single volunteer who flagged it in the ‘Talk’ section.

Eight of the grade B candidates, shown in Fig. 8, and more among the grade C ones, have a disk galaxy as lens. Disk galaxies represent a minority among all lenses and most of the pre-

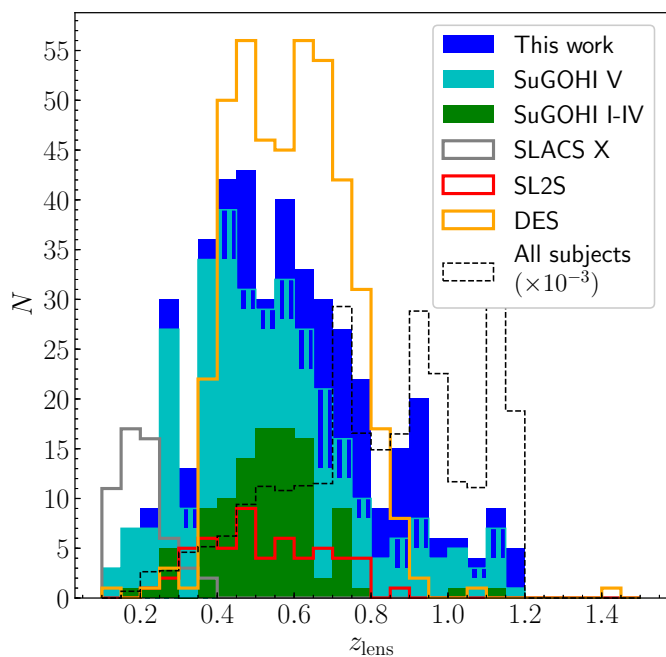


Fig. 6. *Shaded region:* distribution in lens photometric redshift of all grade A and B SuGOHI lenses. The blue portion of the histogram corresponds to lenses discovered in this study. The green part indicates BOSS galaxy lenses discovered with YATTALENS, presented in Paper I, II and IV (Sonnenfeld et al. 2018; Wong et al. 2019; Chan et al. 2019). The cyan part shows lenses discovered by means of visual inspection of galaxy clusters, presented in Paper V. The striped regions indicate lenses discovered independently in this study and in the study of Paper V. Grey solid lines: distribution in lens spectroscopic redshift of lenses from the Sloan ACS Lens Survey (SLACS Auger et al. 2010). Red solid lines: distribution in lens spectroscopic redshift of lenses from the SL2S Survey (Sonnenfeld et al. 2013a,b, 2015). Orange solid lines: distribution in lens photometric redshift of likely lenses discovered in DES by Jacobs et al. (2019b). *Dashed lines:* distribution in photometric redshift of all subjects examined in this study, rescaled down by a factor of 1,000.

viously studied ones are at a lower redshift compared to the average of our sample (but see Suyu et al. 2012, for an exception). The largest sample of disk lenses studied so far is the Sloan WFC Edge-n Late-type Lens Survey (SWELLS Treu et al. 2011), which consists of 19 lenses at $z < 0.3$. Our newly discovered disk lenses extend this family of objects to higher redshift, and, with appropriate follow-up observations, could be used to study the evolution in the mass structure of disks⁹.

Most of the lensed sources in our sample have blue colours. This is related to the fact that the typical source redshift is in the range $1 < z < 3$ (see e.g. Sonnenfeld et al. 2019), close to the peak of cosmic star formation activity. Nevertheless, we were able to discover a limited number of lenses with a red background source. Two of them were classified as grade B candidates and are shown in Fig. 9. The object on the left has a standard fold configuration and was conservatively given a grade B only because one of the images is barely detected in the data. However, it was not classified as lens by the volunteers (although the final value of $P(\text{LENS}|\mathbf{d})$ is higher than the prior probability). Our training sample consisted almost exclusively of blue sources: it is then possible that the volunteers were not ready to recognise such an unusual lens (although past crowdsourcing ex-

⁹ Although the mass within the Einstein radius of these systems is likely dominated by the bulge

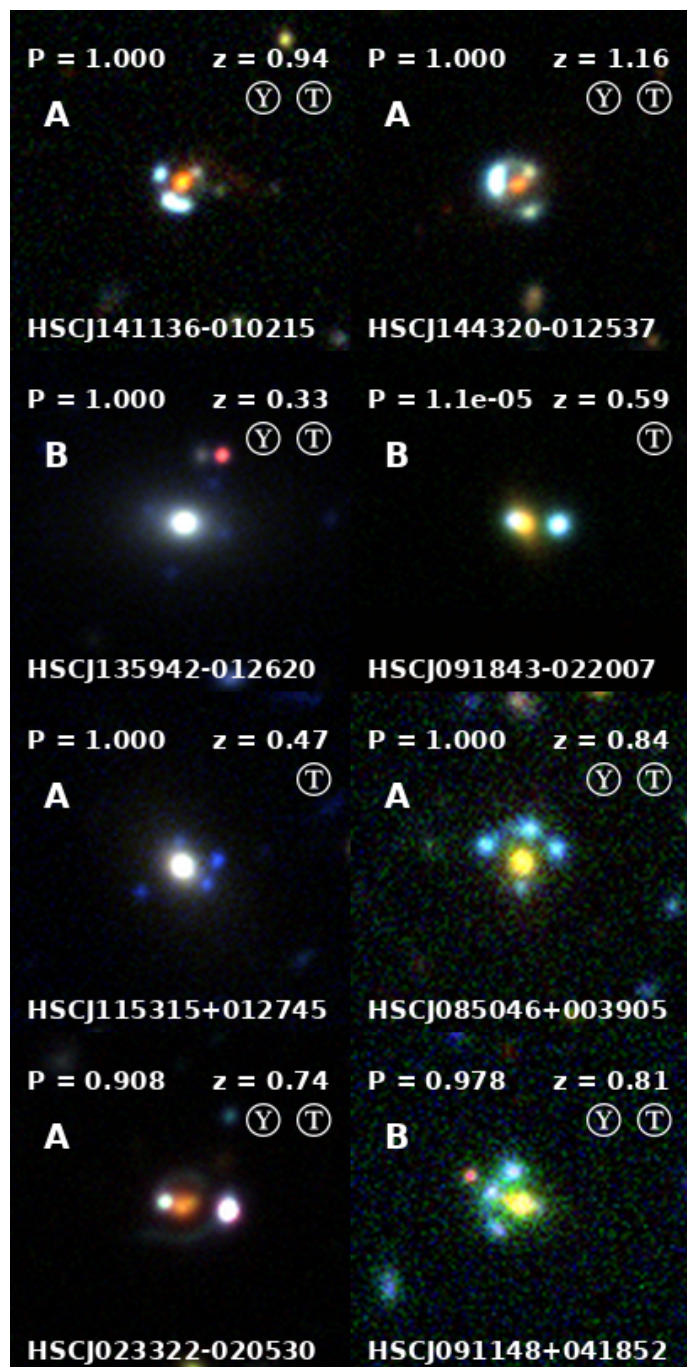


Fig. 7. Set of eight lenses associated with a compact lensed source. In each panel, we show the probability of the subject of being a lens, according to the volunteer classification data (top left), the lens galaxy photo- z (top right), the final grade after our inspection (left). The circled ‘Y’ and ‘T’ on the right, if present, indicate that the candidate was discovered by YATTALENS and was noticed by us in the ‘Talk’ section of the Space Warps website, respectively.

periments proved otherwise Geach et al. 2015). We included it in the sample after it was flagged by one volunteer in the ‘Talk’ section. Both lenses in Fig. 9 were missed by YATTALENS, as it was set up to discard red arcs in order to eliminate contaminants in the form of neighbouring tangentially aligned galaxies.

Finally, we point out how roughly half of our grade C lens candidates consist of systems with either a single visible arc, the counter-image of which, if present, is very close to the centre

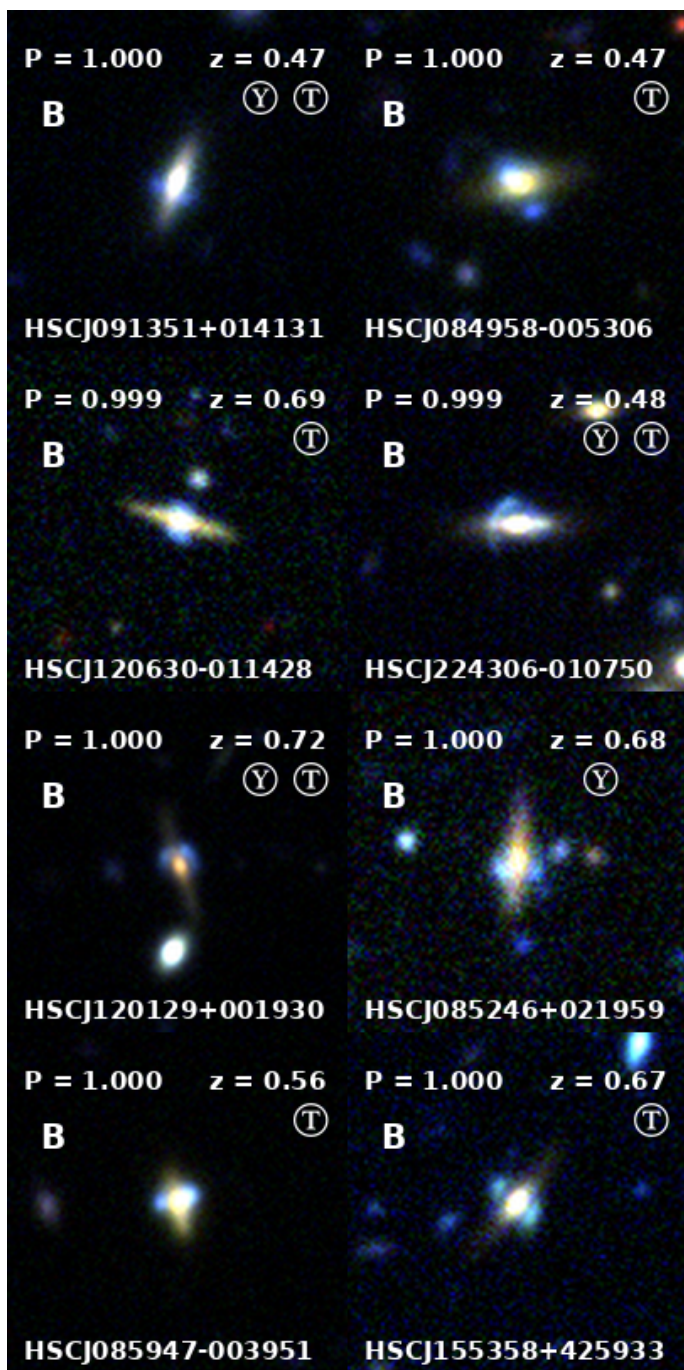


Fig. 8. Set of eight disk galaxy lens candidates discovered in our sample.

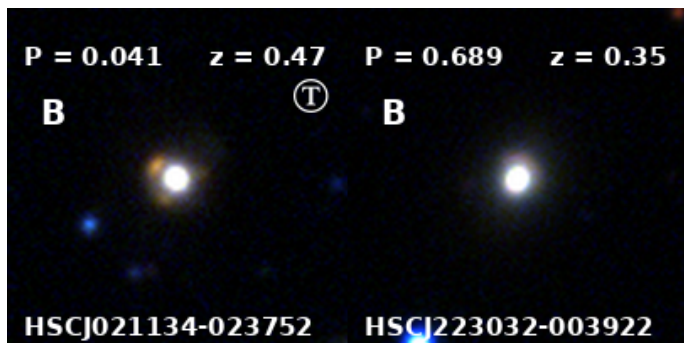


Fig. 9. Two lens candidates with strongly lensed red sources.

and not detected, or a double in a highly asymmetric configuration. It is very difficult to determine whether such candidates are lenses or not using photometric data alone, but, given their abundance (a few hundred in the whole sample), they constitute a very interesting category of lenses: even if only a fraction of them turned out to be real lenses, they would end up dominating the lens population. This is not surprising, but is to be expected from the simple geometrical arguments that we made when describing our procedure for simulating lenses, in subsection 3.1.1: the area in the source plane that gets mapped into highly asymmetric image configurations is larger than the area corresponding to configurations close to symmetric¹⁰.

In Fig. 10, we show a collection of some of the best examples of highly asymmetric doubles that we were able to discover. The figure highlights the importance of the foreground light subtraction step, which, although far from perfect (large negative residuals are typically left in the centre of the image), helps greatly in the detection of faint counter-images close to the centre. Such asymmetric systems are interesting because they allow constraints to be put on the mass in the very inner regions of a lens, dominated by the stars and with a possible contribution from the central supermassive black hole, even in cases when a counter-image is not detected (Smith et al. 2018, 2019). Incidentally, Fig. 10 also illustrates the difficulty in assigning consistent grades to large samples of lens candidates: the object in the top left was given a grade B, in accordance to the criteria discussed in subsection 4.3, while all the other ones were assigned a grade C despite having a very similar image configuration. In our past searches, we used to collectively re-discuss lens candidate grades on a one-by-one basis, after a first round of inspection. This, however, was not feasible in the present study due to the large data volume.

5. Discussion

5.1. Performance of different lens finding methods

The two most important quantities that define the performance of a lens finding method are completeness and purity. The former is the fraction of strong lenses among the ones present in the surveyed sample that are recovered by the method, while the latter is the fraction of objects among the ones labelled as strong lenses that are indeed lenses. Unfortunately, it is very difficult to determine either of them in an absolute sense: it would require to apply our lens finding methods to a large complete sample of real lenses and to a large sample of galaxies representative of our survey the nature of which is known exactly. We can however evaluate the relative performance between our two methods, crowdsourcing and YATTALENS. The data reported in Table 1 shows clearly how the former outperformed the latter both in terms of completeness, with roughly twice the number of lens candidates with grade C or higher, and purity, with 40% of the inspected candidates having grade C or higher, against only 5% for YATTALENS. The comparison is not entirely fair: first of all, YATTALENS correctly identified most of the 52 known lenses used in the training sample, which have been excluded from the summary of Table 1 and would have otherwise increased the completeness of YATTALENS (many of these lenses belong to the sample of lenses discovered with YATTALENS by Sonnenfeld et al. 2018). Secondly, 3,800 duds initially found by YATTALENS were

¹⁰ The picture is complicated by magnification effects: more symmetric configurations correspond in general to a higher magnification, allowing to detect fainter sources in a flux-limited survey. The net effect depends on the slope of the source luminosity function.

removed from the subject sample and only shown to the volunteers as training images, making their classification job slightly easier. However, given the relatively good performance of the volunteers on the training subjects, with only $\sim 10\%$ of the duds being classified as lenses (see Fig. 5), the purity of the sample produced by the volunteers would only have changed by a small margin by including the duds.

Most of the lens candidates missed by YATTALENS were discarded at the arc detection step, for various reasons: their lensed images are either point-like (as two of the candidates shown in Fig. 7), or too red (as in the two cases shown in Fig. 9), or consist of arcs that are considered too faint or too far from the lens galaxy by YATTALENS. In principle, we could adjust the settings of YATTALENS to be able to detect such lenses in future searches, although most likely by paying a penalty in terms of purity.

In the previous section, we also reported the discovery of a number of highly probable lenses that were flagged by volunteers in the ‘Talk’ section of Space Warps, including some that were missed by both the volunteer classification data and YATTALENS. Based on the numbers reported in Table 1, with as many as 11 grade A and 86 grade B lens candidates found among 264 inspected candidates, one could be inclined to conclude that the ‘Talk’ section provides much purer samples compared to the analysis of classification data. However, those numbers are misleading: 264 were the candidates that were deemed sufficiently interesting to be included in the final grading step, and were selected after sorting through thousands of subjects flagged by volunteers. The effective purity of this lens search method is therefore much lower than Table 1 suggests.

5.2. Comparison with the Metcalf et al. (2019) lens finding challenge

Metcalf et al. (2019) carried out a lens finding challenge, in which 100,000 simulated images of lenses and non-lenses were classified with a variety of lens finding methods over the course of 48 hours. Among the lens finders that took part in the challenge, there were several machine learning-based methods, a visual inspection effort and a simplified version of YATTALENS, dubbed YATTALENS LITE, limited to the arc-finding step and stripped of the modelling part to meet the time constraints of the challenge. The methods with the best performance were based on machine learning. YATTALENS LITE achieved a false positive rate of $\sim 10\%$ and a true positive rate (i.e. the fraction of lenses correctly classified as such over the total number of lenses inspected) of 75%, while the performance of visual inspection was marginally better.

The performance of YATTALENS on the real data used in this work is different from that of YATTALENS LITE on the lens finding challenge. We achieved a false positive rate of $\approx 2\%$ (given by the number of grade 0 candidates classified as lenses by YATTALENS, 6,470, among the 300,000 scanned subjects). This lower value can be explained partly by the presence of the modelling step, which was skipped in the lens finding challenge and which typically brings an improvement in purity of a factor of 3, and partly by the different composition of the non-lens sample of the challenge, compared to the sample of real galaxies. The true positive rate is also lower in this experiment: although we do not know the total number of lenses present among all scanned subjects, we can obtain an upper limit on the true positive rate by dividing the number of grade A and B candidates recovered by YATTALENS ($6 + 68 = 74$) by the total number of grade A and B candidates found ($14 + 130 = 144$), roughly 50% (this fraction increases if we also consider the 52 real lenses used as training

subjects, but is still below the 75% true positive rate scored in the lens finding challenge). As for the false positive rate, the true positive rate is also sensitive to the details of the distribution of lens properties in the sample: for example, we suspect that the lens finding challenge had a higher fraction of lenses that would be classified as ‘easy’ according to our definition, boosting the true positive rate. The main lesson from this comparison is that, while lens finding challenges carried out on simulated data can be very useful tests of lens finding methods, results can vary a lot depending on the details of the test samples used. Therefore, tests on real data are essential to accurately assess the performance of a given lens finding method. These are not a viable option at the moment, due to the relatively low number of known lenses, but might become feasible in the future.

5.3. Lens finding efficiency dependence on image depth

One of the most important aspects of photometric data for lens finding purposes is image depth: in principle, deeper data should allow the detection of fainter background sources, and therefore more lenses. The data used for our study, taken from the S17A internal data release of HSC, span a wide range in depth: the number of individual exposures that make up the coadded images used for our analysis goes from a minimum of one to the survey standard value of six in i -band, and even more in regions where multiple pointings overlap. We can then check whether the number density of lens candidates correlates with image depth. In Fig. 11 we plot the distribution in i - and g -band sky background fluctuation of all subjects, of grade A and B lens candidates combined, and of grade C ones. By looking at the i -band distribution (left panel), we can see how the distribution of grade A and B candidates is shifted towards lower levels of background noise compared to the distribution of all subjects. A Kolmogorov-Smirnov test reveals a p-value of 8.8×10^{-4} , hence a low probability that the two samples (all subjects and grade A, B candidates) are drawn from the same distribution. While the i -band data confirms the idea that deeper data leads to a higher number of detected lenses, the g -band distribution appears to tell a different story: there is no obvious difference between the distribution in background fluctuation of lens candidates and all subjects, with the Kolmogorov-Smirnov test giving a p-value of 0.16. Given that the g -band is, for the vast majority of our candidates, the one with the highest contrast between lens and source, we would have expected an even higher difference between the two distributions. This result instead suggests that g -band depth is probably not the limiting factor in our lens finding campaign, but i -band depth is more important. This could be related to the foreground light subtraction step, for which we rely on the i -band image to obtain a model for the surface brightness profile of the lens.

5.4. Comparison with past crowdsourcing experiments

This was the third crowd-sourced lens finding experiment carried out by Space Warps, after the search on CFHT-LS data (Marshall et al. 2016; More et al. 2016) and on the VISTA-CFHT Stripe 82 survey (Geach et al. 2015). More et al. (2016) were able to find 91 probable lenses, 29 of which were previously unknown, in 160 square degrees of data. The number density of grade A and B lenses found in the present search is similar, though it is hard to make a quantitative comparison, due to different definitions of what constitutes a probable lens candidate and to the fact that we excluded known lenses from our sub-

ject sample from the start. An essential difference between the present study and the CFHT-LS Space Warps campaign is that this was a targeted search: we looked for lenses only among a set of galaxies in a given redshift and stellar mass range. The search carried out by More et al. (2016) instead consisted of two stages: a blind search over tiles of the whole survey area, followed by a re-inspection of the most promising candidates. Compared to the More et al. (2016) study, we found a much larger fraction of ‘undecided’ subjects, for which their probability of being a lens did not converge neither to a value close to unity nor to very low values, retired from the sample only after reaching the maximum allowed number of classifications. We think this to be a consequence of the fact that volunteers have been able to detect fainter lens-like features, that are intrinsically more difficult to classify, compared to the CFHT-LS campaign. There are a few reasons for this. First of all, the chances of finding faint arcs are higher in a targeted search, when the attention is focused on a well defined object, as opposed to a blind search. Secondly, HSC data is deeper than CFHT-LS, increasing the number density of fainter features in the vicinity of a foreground galaxy. Thirdly, the presence of foreground-subtracted images in our experiment allows the identification of lenses with a lower contrast between source and lens light. These factors lead to a higher fraction of ambiguous lens candidates in our sample.

6. Conclusions

We carried out a crowdsourced lens search over 442 square degrees of data from the HSC survey. The search was carried out on a sample of $\sim 300,000$ galaxies with photometric redshift between 0.2 and 1.2 and a stellar mass larger than $10^{11.2} M_{\odot}$. Almost 6,000 citizen volunteers participated in the crowdsourcing experiment, named Space Warps - HSC. We collected ~ 2.5 million classifications, which we then analysed with an algorithm developed in past editions of Space Warps. In parallel, we searched for lenses in the same sample of galaxies using the automated lens finding method YATTALENS. From the two searches combined, we found 143 highly probable (grade A or B) new lens candidates, in an area that already included 70 known lenses. Compared to YATTALENS, crowdsourcing was by far the most successful lens finding method, both in terms of completeness and purity. We found lenses of a variety of kinds, including lenses with a compact source, with a red source, group-scale lenses and lens candidates with highly asymmetric configurations.

In the coming years, the volume of data available for lens finding purposes will increase greatly, as the Euclid space telescope¹¹ and the Large Synoptic Survey Telescope¹² (LSST) are each planned to cover areas of the sky that are more than a factor of thirty larger than that scanned in our study. Scaling up Space Warps to such data volumes will be challenging: a much larger number of volunteers and/or a higher number of classification per volunteer will be needed. We can aim to improve the efficiency of our search by modifying the definition of the parent sample of subjects passed to the volunteers. For instance, machine learning-based methods could potentially be used to pre-select large samples of possible lenses that are then refined in a visual inspection step via crowdsourcing. Nevertheless, our experiment shows how crowdsourcing is a very powerful tool for finding lenses, delivering samples of lens candidates with relatively high purity and completeness, and we expect it to play

a major role in lens finding in the 2020s. YATTALENS can produce samples of roughly one grade C lens candidate or better per square degree in HSC-like data, and is therefore confirmed to be a valid tool for finding galaxy-scale lenses in a semi-automated way, provided that high completeness is not a critical requirement.

Acknowledgements. We thank all of the volunteers who participated in Space Warps - HSC, whose Zooniverse usernames are listed at the end of <https://www.zooniverse.org/projects/aprajita/space-warps-hsc/about/team>, with particular thanks to Ivan A. Terentev for flagging the lens HSCJ021134–023752 and many other good candidates. We thank all of the Science Friday Team (in particular Ariel Zych, Christopher Intagliata, Brandon Echter and Ira Flatow) for featuring the SW-HSC project in two broadcasts, that greatly enhanced and promoted the project to a wider community. We also thank Michael Laraia, Hugh Dickinson and Lucy Fortson (University of Minnesota) for their implementation of the Space Warps Analysis Pipeline for the PANOPTES Zooniverse platform and integration with CAESAR functionality. AS acknowledges funding from the European Union’s Horizon 2020 research and innovation programme under grant agreement No 792916, as well as a KAKENHI Grant from the Japan Society for the Promotion of Science (JSPS), MEXT, Number JP17K14250. ATJ is supported by JSPS KAKENHI Grant number JP17H02868. JHHC acknowledges support from the Swiss National Science Foundation (SNSF). This work was supported by World Premier International Research Center Initiative (WPI Initiative), MEXT, Japan. The Hyper Suprime-Cam (HSC) collaboration includes the astronomical communities of Japan and Taiwan, and Princeton University. The HSC instrumentation and software were developed by the National Astronomical Observatory of Japan (NAOJ), the Kavli Institute for the Physics and Mathematics of the Universe (Kavli IPMU), the University of Tokyo, the High Energy Accelerator Research Organization (KEK), the Academia Sinica Institute for Astronomy and Astrophysics in Taiwan (ASIAA), and Princeton University. Funding was contributed by the FIRST programme from Japanese Cabinet Office, the Ministry of Education, Culture, Sports, Science, and Technology (MEXT), the Japan Society for the Promotion of Science (JSPS), Japan Science and Technology Agency (JST), the Toray Science Foundation, NAOJ, Kavli IPMU, KEK, ASIAA, and Princeton University. Funding for SDSS-III has been provided by the Alfred P. Sloan Foundation, the Participating Institutions, the National Science Foundation, and the U.S. Department of Energy Office of Science. The SDSS-III web site is <http://www.sdss3.org/>. SDSS-III is managed by the Astrophysical Research Consortium for the Participating Institutions of the SDSS-III Collaboration including the University of Arizona, the Brazilian Participation Group, Brookhaven National Laboratory, Carnegie Mellon University, University of Florida, the French Participation Group, the German Participation Group, Harvard University, the Instituto de Astrofísica de Canarias, the Michigan State/Notre Dame/JINA Participation Group, Johns Hopkins University, Lawrence Berkeley National Laboratory, Max Planck Institute for Astrophysics, Max Planck Institute for Extraterrestrial Physics, New Mexico State University, New York University, Ohio State University, Pennsylvania State University, University of Portsmouth, Princeton University, the Spanish Participation Group, University of Tokyo, University of Utah, Vanderbilt University, University of Virginia, University of Washington, and Yale University.

References

- Aihara, H., Arimoto, N., Armstrong, R., et al. 2018, PASJ, 70, S4
 Auger, M. W., Treu, T., Gavazzi, R., et al. 2010, ApJ, 721, L163
 Axelrod, T., Kantor, J., Lupton, R. H., & Pierfederici, F. 2010, in Proc. SPIE, Vol. 7740, Software and Cyberinfrastructure for Astronomy, 774015
 Barnabè, M., Spiniello, C., Koopmans, L. V. E., et al. 2013, MNRAS, 436, 253
 Bertin, E. & Arnouts, S. 1996, A&AS, 117, 393
 Bolton, A. S., Brownstein, J. R., Kochanek, C. S., et al. 2012, ApJ, 757, 82
 Bosch, J., Armstrong, R., Bickerton, S., et al. 2018, PASJ, 70, S5
 Chan, J. H. H., Suyu, S. H., Sonnenfeld, A., et al. 2019, arXiv e-prints, arXiv:1911.02587
 Dark Energy Survey Collaboration, Abbott, T., Abdalla, F. B., et al. 2016, MNRAS, 460, 1270
 Dawson, K. S., Schlegel, D. J., Ahn, C. P., et al. 2013, AJ, 145, 10
 de Jong, J. T. A., Verdoes Kleijn, G. A., Boxhoorn, D. R., et al. 2015, A&A, 582, A62
 Erben, T., Hildebrandt, H., Miller, L., et al. 2013, MNRAS, 433, 2545
 Geach, J. E., More, A., Verma, A., et al. 2015, MNRAS, 452, 502
 Grillo, C., Rosati, P., Suyu, S. H., et al. 2018, ApJ, 860, 94
 Hildebrandt, H., Erben, T., Kuijken, K., et al. 2012, MNRAS, 421, 2355
 Hsueh, J.-W., Enzi, W., Vegetti, S., et al. 2019, arXiv e-prints, arXiv:1905.04182

¹¹ <https://euclid-ec.org/>

¹² <https://lsst.org>

- Huang, X., Domingo, M., Pilon, A., et al. 2019, arXiv e-prints, arXiv:1906.00970
- Ivezić, Ž., Kahn, S. M., Tyson, J. A., et al. 2008, arXiv e-prints [arXiv:0805.2366]
- Jacobs, C., Collett, T., Glazebrook, K., et al. 2019a, ApJS, 243, 17
- Jacobs, C., Collett, T., Glazebrook, K., et al. 2019b, ApJS, 243, 17
- Jaelani, A. T., More, A., Oguri, M., et al. 2020, arXiv e-prints, arXiv:2002.01611
- Jaelani, A. T., More, A., Sonnenfeld, A., et al. 2019, arXiv e-prints, arXiv:1909.00120
- Jurić, M., Kantor, J., Lim, K., et al. 2015, ArXiv e-prints [arXiv:1512.07914]
- Koopmans, L. V. E. & Treu, T. 2003, ApJ, 583, 606
- Kormann, R., Schneider, P., & Bartelmann, M. 1994, A&A, 284, 285
- Mao, S. & Schneider, P. 1998, MNRAS, 295, 587
- Marshall, P. J., Verma, A., More, A., et al. 2016, MNRAS, 455, 1171
- Mediavilla, E., Muñoz, J. A., Falco, E., et al. 2009, ApJ, 706, 1451
- Metcalfe, R. B., Meneghetti, M., Avestruz, C., et al. 2019, A&A, 625, A119
- Millon, M., Galan, A., Courbin, F., et al. 2019, arXiv e-prints, arXiv:1912.08027
- Miyazaki, S., Komiyama, Y., Kawanomoto, S., et al. 2018, PASJ, 70, S1
- More, A., Lee, C.-H., Oguri, M., et al. 2017, MNRAS, 465, 2411
- More, A., McKean, J. P., More, S., et al. 2009, MNRAS, 394, 174
- More, A., Verma, A., Marshall, P. J., et al. 2016, MNRAS, 455, 1191
- Newman, A. B., Ellis, R. S., & Treu, T. 2015, ApJ, 814, 26
- Oguri, M., Rusu, C. E., & Falco, E. E. 2014, MNRAS, 439, 2494
- Oldham, L. J. & Auger, M. W. 2018, MNRAS, 476, 133
- Petrillo, C. E., Tortora, C., Vernardos, G., et al. 2019a, MNRAS, 484, 3879
- Petrillo, C. E., Tortora, C., Vernardos, G., et al. 2019b, MNRAS, 484, 3879
- Ruff, A. J., Gavazzi, R., Marshall, P. J., et al. 2011, ApJ, 727, 96
- Schechter, P. L., Pooley, D., Blackburne, J. A., & Wambsganss, J. 2014, ApJ, 793, 96
- Smith, R. J., Collier, W. P., Ozaki, S., & Lucey, J. R. 2019, arXiv e-prints, arXiv:1911.06338
- Smith, R. J., Lucey, J. R., & Collier, W. P. 2018, MNRAS, 481, 2115
- Smith, R. J., Lucey, J. R., & Conroy, C. 2015, MNRAS, 449, 3441
- Sonnenfeld, A., Chan, J. H. H., Shu, Y., et al. 2018, PASJ, 70, S29
- Sonnenfeld, A., Gavazzi, R., Suyu, S. H., Treu, T., & Marshall, P. J. 2013a, ApJ, 777, 97
- Sonnenfeld, A., Jaelani, A. T., Chan, J., et al. 2019, A&A, 630, A71
- Sonnenfeld, A., Treu, T., Gavazzi, R., et al. 2012, ApJ, 752, 163
- Sonnenfeld, A., Treu, T., Gavazzi, R., et al. 2013b, ApJ, 777, 98
- Sonnenfeld, A., Treu, T., Marshall, P. J., et al. 2015, ApJ, 800, 94
- Spiniello, C., Trager, S. C., Koopmans, L. V. E., & Chen, Y. P. 2012, ApJ, 753, L32
- Suyu, S. H., Bonvin, V., Courbin, F., et al. 2016, ArXiv e-prints [arXiv:1607.00017]
- Suyu, S. H., Hensel, S. W., McKean, J. P., et al. 2012, ApJ, 750, 10
- Tanaka, M. 2015, ApJ, 801, 20
- Tanaka, M., Coupon, J., Hsieh, B.-C., et al. 2018, PASJ, 70, S9
- Treu, T., Auger, M. W., Koopmans, L. V. E., et al. 2010, ApJ, 709, 1195
- Treu, T., Dutton, A. A., Auger, M. W., et al. 2011, MNRAS, 417, 1601
- Treu, T. & Koopmans, L. V. E. 2002, ApJ, 575, 87
- Vegetti, S., Koopmans, L. V. E., Bolton, A., Treu, T., & Gavazzi, R. 2010, MNRAS, 408, 1969
- Wong, K. C., Sonnenfeld, A., Chan, J. H. H., et al. 2018, ApJ, 867, 107
- Wong, K. C., Suyu, S. H., Chen, G. C. F., et al. 2019, arXiv e-prints, arXiv:1907.04869

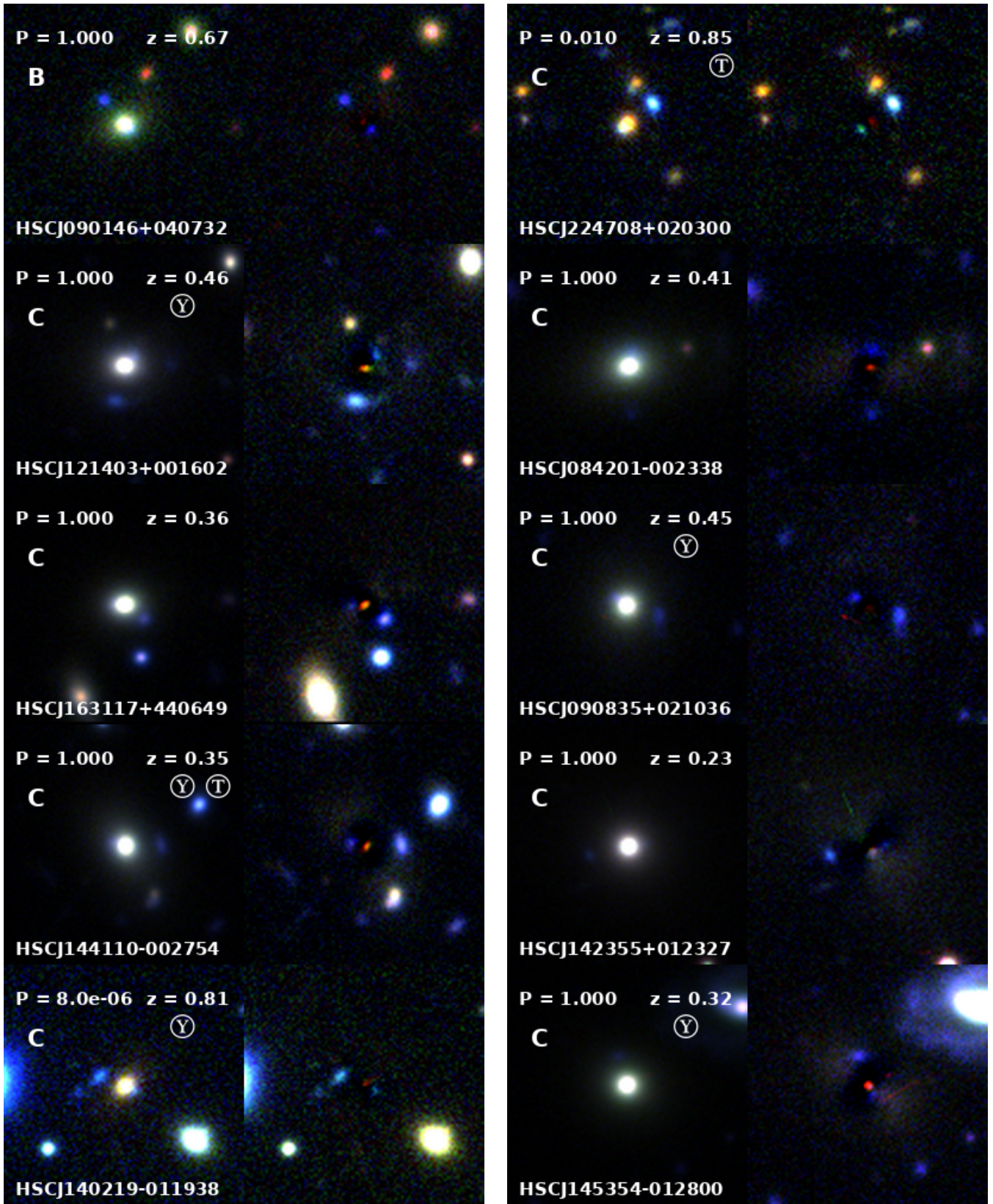


Fig. 10. Selected sample of ten lens candidates with a highly asymmetric image configuration. In each row, the left panel shows the original image, while the right one shows the foreground-subtracted one.

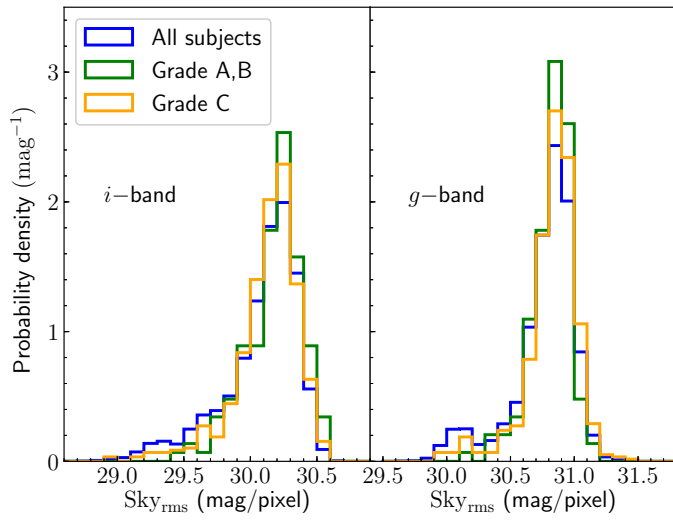


Fig. 11. Distribution in sky background rms (in AB magnitudes per pixel) of all subjects, grade A and B candidates combined and grade C candidates, in *i*- (left) and *g*-band (right).

Table 2. Grade A and B lens candidates. Columns 7 and 8 indicate whether the candidate was found by YATTALENS or was noted from the ‘Talk’ section of the Space Warps website. Column 9 lists references to papers that include the same lens candidate (and that were published after the beginning of the Space Warps - HSC campaign), as follows: ¹Jaelani et al. (2020), ²Chan et al. (2019), ³Petrillo et al. (2019a), ⁴Jacobs et al. (2019a), ⁵Huang et al. (2019)

Name	R.A. (deg)	Dec. (deg)	z_{phot}	Grade	P(LENS d)	YL	Talk	References
HSCJ015913-054320	29.8056	-5.7224	0.93	B	1.00	N	N	...
HSCJ015938-035859	29.9092	-3.9831	1.16	B	0.80	N	N	1
HSCJ020018-030549	30.0771	-3.0971	0.77	B	1.00	Y	Y	...
HSCJ020050-030027	30.2097	-3.0075	0.73	B	1.00	N	Y	...
HSCJ020449-020206	31.2078	-2.0350	0.85	B	1.00	N	Y	...
HSCJ020810-022018	32.0445	-2.3384	0.63	B	1.00	Y	Y	...
HSCJ020816-023724	32.0671	-2.6234	0.48	B	1.00	N	N	1
HSCJ020955-024442	32.4809	-2.7451	0.72	B	1.00	Y	Y	1
HSCJ021134-023752	32.8928	-2.6312	0.47	B	4.00×10^{-2}	N	Y	...
HSCJ021408-020628	33.5333	-2.1079	0.70	B	1.00	N	Y	1,4
HSCJ021645-020835	34.1890	-2.1431	0.61	B	1.00	N	Y	...
HSCJ021829-034040	34.6216	-3.6780	0.89	B	1.00	Y	Y	...
HSCJ022422-014946	36.0931	-1.8296	0.61	B	1.00	Y	Y	...
HSCJ023038-015248	37.6589	-1.8803	0.40	B	1.00	N	Y	...
HSCJ023133-042501	37.8900	-4.4171	0.92	B	1.80×10^{-4}	N	Y	...
HSCJ023150-020509	37.9617	-2.0859	0.76	B	1.00	N	Y	1
HSCJ023305-022836	38.2733	-2.4767	0.58	A	1.00	Y	N	1
HSCJ023322-020530	38.3444	-2.0918	0.74	A	0.91	Y	Y	1
HSCJ023331-032801	38.3831	-3.4670	1.12	B	0.98	Y	N	1
HSCJ023629-060449	39.1216	-6.0804	0.91	B	1.00	N	Y	...
HSCJ084211+013835	130.5465	1.6432	0.28	B	1.00	Y	N	3
HSCJ084520-005456	131.3340	-0.9156	0.34	A	1.00	N	Y	1,3
HSCJ084536-000456	131.4002	-0.0825	0.81	B	1.00	Y	Y	...
HSCJ084958-005306	132.4954	-0.8851	0.47	B	1.00	N	Y	...
HSCJ085046+003905	132.6942	0.6515	0.84	A	1.00	Y	Y	...
HSCJ085246+021959	133.1949	2.3333	0.68	B	1.00	Y	N	...
HSCJ085842-002745	134.6764	-0.4627	0.61	B	1.00	N	Y	1
HSCJ085947-003951	134.9484	-0.6644	0.56	B	1.00	N	Y	...
HSCJ090146+040732	135.4428	4.1256	0.67	B	1.00	N	N	...
HSCJ090241+025318	135.6713	2.8884	0.92	B	1.00	Y	Y	...
HSCJ090404+012516	136.0180	1.4211	0.82	B	1.00	N	Y	1
HSCJ090502+004424	136.2604	0.7400	0.74	B	1.00	Y	Y	...
HSCJ090548+004743	136.4533	0.7954	0.93	B	1.00	N	N	...
HSCJ090611+011951	136.5460	1.3310	0.65	B	1.00	N	Y	1
HSCJ090618+003053	136.5789	0.5150	0.88	B	1.00	Y	N	...
HSCJ090707-004741	136.7795	-0.7948	0.76	B	0.72	N	N	...
HSCJ090754+005732	136.9765	0.9590	0.68	A	1.00	N	Y	1
HSCJ090806+011955	137.0261	1.3321	0.65	B	1.00	Y	Y	1
HSCJ090822-010752	137.0930	-1.1312	0.77	B	1.00	Y	Y	...
HSCJ090938+002842	137.4108	0.4785	0.74	B	1.00	Y	Y	...
HSCJ091031+003142	137.6317	0.5286	0.25	B	1.00	Y	Y	...
HSCJ091033+000712	137.6381	0.1200	0.48	B	0.77	N	N	...
HSCJ091148+041852	137.9538	4.3147	0.81	B	0.98	Y	Y	...
HSCJ091351+014131	138.4663	1.6921	0.47	B	1.00	Y	Y	...
HSCJ091413-002444	138.5561	-0.4123	0.75	B	1.00	Y	N	...
HSCJ091740+004438	139.4203	0.7439	0.31	B	1.00	Y	N	...
HSCJ091843-022007	139.6808	-2.3354	0.59	B	1.10×10^{-5}	N	Y	...
HSCJ092120+044430	140.3365	4.7418	0.59	B	1.00	N	Y	...
HSCJ092136+021409	140.4028	2.2360	0.34	B	1.00	Y	Y	1
HSCJ092545+001702	141.4375	0.2841	0.76	B	1.00	Y	Y	1
HSCJ114233+004607	175.6390	0.7686	0.61	B	1.00	N	Y	...
HSCJ114438-002547	176.1619	-0.4297	0.70	B	1.00	Y	Y	1
HSCJ114444+001344	176.1874	0.2291	0.92	B	1.00	N	Y	...
HSCJ114445+005256	176.1898	0.8824	0.72	B	1.00	N	N	...
HSCJ115011-002019	177.5469	-0.3388	0.65	B	1.00	Y	Y	...
HSCJ115057-015316	177.7392	-1.8880	0.94	B	5.00×10^{-6}	N	Y	...

Table 2. continued.

Name	R.A. (deg)	Dec. (deg)	z_{phot}	Grade	P(LENS d)	YL	Talk	References
HSCJ115315+012745	178.3150	1.4628	0.47	A	1.00	N	Y	1
HSCJ115529-004255	178.8727	-0.7155	0.82	B	1.00	N	N	...
HSCJ115630-020027	179.1289	-2.0077	1.15	B	1.00×10^{-6}	N	Y	...
HSCJ120053-013357	180.2220	-1.5661	0.92	B	1.00	Y	Y	...
HSCJ120109+003330	180.2911	0.5583	1.11	B	1.00	Y	Y	...
HSCJ120111+012635	180.2980	1.4431	0.59	B	1.00	N	Y	...
HSCJ120129+001930	180.3716	0.3250	0.72	B	1.00	Y	Y	...
HSCJ120141+012736	180.4248	1.4603	0.75	B	0.16	N	Y	...
HSCJ120256+003930	180.7369	0.6585	0.72	A	1.00	N	N	1
HSCJ120630-011428	181.6291	-1.2413	0.69	B	1.00	N	Y	...
HSCJ120806-012233	182.0275	-1.3759	0.36	B	1.00	Y	N	...
HSCJ120849+012845	182.2052	1.4792	0.99	B	1.00	Y	Y	1
HSCJ120855-010304	182.2305	-1.0513	0.64	B	0.93	N	N	1
HSCJ135942-012620	209.9285	-1.4391	0.33	B	1.00	Y	Y	1
HSCJ140042-010556	210.1785	-1.0991	0.70	B	1.00	Y	Y	...
HSCJ140452+005122	211.2179	0.8563	0.33	B	1.00	Y	N	3
HSCJ140753-002816	211.9734	-0.4713	0.44	B	1.00	N	Y	1
HSCJ141050-010938	212.7088	-1.1607	0.63	B	1.00	N	Y	1
HSCJ141105+002532	212.7741	0.4257	1.13	B	1.00	N	N	1
HSCJ141136-010215	212.9022	-1.0377	0.94	A	1.00	Y	Y	...
HSCJ141137+010720	212.9073	1.1223	0.44	B	1.00	Y	Y	1,3
HSCJ141420-013646	213.5874	-1.6128	0.49	A	1.00	N	Y	3
HSCJ141435-001601	213.6483	-0.2671	0.71	B	1.00	N	N	...
HSCJ141558+523955	213.9926	52.6654	0.45	B	1.00	Y	N	...
HSCJ141646-011813	214.1941	-1.3037	0.66	B	1.00	N	N	...
HSCJ141649+013822	214.2076	1.6395	0.33	B	1.00	Y	Y	...
HSCJ141805+004435	214.5232	0.7432	0.85	B	1.00	N	Y	1
HSCJ141908+002049	214.7852	0.3472	0.25	B	1.00	N	Y	1
HSCJ141933+010223	214.8888	1.0399	1.12	B	1.00	Y	N	...
HSCJ142017+005831	215.0742	0.9755	0.25	B	1.00	Y	N	1
HSCJ142018+005832	215.0751	0.9758	0.78	B	0.69	N	N	...
HSCJ142031+002021	215.1311	0.3392	0.46	B	1.00	N	Y	...
HSCJ142103+002219	215.2654	0.3720	0.64	B	1.00	Y	N	1,5
HSCJ142149-002403	215.4578	-0.4008	0.58	B	1.00	N	N	1
HSCJ142232+000134	215.6347	0.0263	0.23	B	1.00	Y	Y	3
HSCJ142234-000225	215.6429	-0.0404	1.05	B	1.00	Y	N	...
HSCJ142336-004034	215.9040	-0.6763	0.88	B	1.00	Y	N	...
HSCJ142602+010842	216.5122	1.1450	0.86	B	1.00	N	N	...
HSCJ142640+000958	216.6693	0.1663	0.59	B	1.00	N	N	...
HSCJ142754+003944	216.9787	0.6624	0.82	B	1.00	N	Y	...
HSCJ142811-005021	217.0486	-0.8392	0.65	B	1.00	Y	Y	...
HSCJ143113-000613	217.8079	-0.1037	0.73	B	1.00	Y	Y	1
HSCJ143150+013019	217.9619	1.5055	0.72	B	1.00	Y	Y	...
HSCJ143243-004553	218.1831	-0.7648	0.45	B	1.00	Y	Y	...
HSCJ143408-001311	218.5372	-0.2199	0.88	B	1.00	Y	N	...
HSCJ143518-012526	218.8287	-1.4239	0.98	B	0.89	N	N	...
HSCJ143519-010636	218.8296	-1.1101	0.76	B	1.00	Y	Y	1
HSCJ143529+001812	218.8714	0.3035	0.60	B	1.00	Y	N	...
HSCJ143901+005117	219.7558	0.8550	0.75	B	1.00	Y	Y	...
HSCJ143917-003917	219.8219	-0.6550	0.71	B	1.00	N	Y	...
HSCJ144101+013344	220.2562	1.5624	0.53	B	1.00	Y	Y	...
HSCJ144132-005358	220.3862	-0.8995	0.49	A	1.00	N	N	...
HSCJ144230-002353	220.6291	-0.3981	0.40	B	1.00	Y	Y	2,3
HSCJ144320-012537	220.8360	-1.4270	1.16	A	1.00	Y	Y	2
HSCJ144603-004016	221.5146	-0.6713	0.23	B	1.00	Y	N	3
HSCJ145020+003535	222.5835	0.5931	1.15	B	4.50×10^{-5}	N	Y	...
HSCJ145217-014714	223.0726	-1.7873	0.47	B	1.00	Y	N	...
HSCJ150021-004936	225.0876	-0.8269	0.41	A	1.00	N	Y	...
HSCJ155358+425933	238.4957	42.9926	0.67	B	1.00	N	Y	...

Table 2. continued.

Name	R.A. (deg)	Dec. (deg)	z_{phot}	Grade	P(LENS d)	YL	Talk	References
HSCJ155619+422854	239.0812	42.4819	1.01	B	1.00	N	N	...
HSCJ155634+432413	239.1452	43.4038	0.69	B	1.00	N	Y	...
HSCJ155806+431702	239.5256	43.2840	0.75	B	1.00	N	Y	...
HSCJ155814+423707	239.5611	42.6188	0.76	B	1.00	Y	Y	...
HSCJ155830+443339	239.6258	44.5610	0.58	B	1.00	Y	N	...
HSCJ155950+424950	239.9599	42.8307	0.76	B	1.00	N	N	...
HSCJ161022+422228	242.5925	42.3747	0.64	B	0.98	Y	N	...
HSCJ161432+435125	243.6362	43.8570	0.92	B	0.87	N	Y	...
HSCJ161818+434527	244.5774	43.7576	0.69	B	0.63	N	Y	1
HSCJ162422+433958	246.0930	43.6661	0.92	B	1.00	Y	N	...
HSCJ221222-001811	333.0950	-0.3031	0.93	B	1.00	Y	Y	1
HSCJ222041+004912	335.1725	0.8201	0.81	B	1.00	N	Y	...
HSCJ222347+004928	335.9475	0.8247	1.16	B	7.00×10^{-6}	N	Y	...
HSCJ222445+010916	336.1891	1.1547	0.76	B	9.00×10^{-6}	N	Y	...
HSCJ222515+004822	336.3161	0.8063	0.28	B	1.00	Y	N	...
HSCJ222638-003449	336.6596	-0.5804	0.36	A	1.00	Y	Y	1
HSCJ222723+003257	336.8465	0.5494	0.85	B	1.00	Y	Y	...
HSCJ223032-003922	337.6342	-0.6561	0.35	B	0.69	N	N	...
HSCJ223200+004015	338.0012	0.6709	0.90	B	1.00	Y	N	...
HSCJ223443+030307	338.6830	3.0522	0.57	B	1.00	Y	Y	...
HSCJ223626-005400	339.1096	-0.9002	0.99	B	1.00	Y	Y	...
HSCJ223735+004014	339.3974	0.6708	0.47	B	1.00	Y	N	...
HSCJ223934+023507	339.8945	2.5853	0.91	A	1.00	N	Y	1
HSCJ224154+000331	340.4776	0.0588	0.58	B	1.00	Y	Y	...
HSCJ224211+023023	340.5485	2.5066	0.75	B	2.90×10^{-4}	N	Y	...
HSCJ224306-010750	340.7789	-1.1308	0.48	B	1.00	Y	Y	...
HSCJ224429-001759	341.1226	-0.2998	0.85	B	1.00	Y	Y	...
HSCJ224758+020648	341.9937	2.1136	0.72	B	0.37	N	Y	...